Supporting information for:

Backbone Deprotonation Defines a Hidden Decomposition Pathway of Diphosphine Ligands

Logan J. Taylor, A. Dina Dilinaer, Paul D. Boyle, and Marcus W. Drover*

*E-mail: marcus.drover@uwo.ca

Department of Chemistry, Western University, 1151 Richmond Street, London, ON, N8K 3G6, Canada

1. Experimental Section:

General considerations. All experiments were carried out in a glovebox under an atmosphere of dry nitrogen employing degassed, dried solvents, unless stated otherwise. Non-halogenated solvents were tested with a standard purple solution of sodium benzophenone ketyl in tetrahydrofuran to confirm effective moisture removal. MeCN was acquired from solvent purification systems (SPS) and stored over 3 Å molecular sieves. Anhydrous and inhibitor free THF and C_6D_6 were purchased from Sigma-Aldrich and used without further purification. All other reagents were purchased from commercial vendors and used without further purification unless otherwise stated. $NaCp^{Me}$ [1] and d*n*ppe[2] were synthesized following literature procedures.

Physical methods. All NMR data were recorded with a Bruker AVIII HD 400 MHz or a Bruker Neo 600 MHz instrument. ^1H NMR spectra are reported in parts per million (ppm) and are referenced to residual solvent e.g., $^1H(C_6D_6)$: $\delta = 7.16$; $^1H(CDCl_3)$: $\delta = 7.26$; coupling constants are reported in Hz. ^{31}P $\{^1H\}$ NMR spectra were performed as proton-decoupled experiments (unless explicitly stated otherwise) and are reported in ppm. Mass spectrometry was carried out with a Orbitrap Exploris 120 mass spectrometer using atmospheric pressure chemical ionization (APCI) or liquid injection field desorption ionization (LIFDI).

2. Preparation of Compounds:

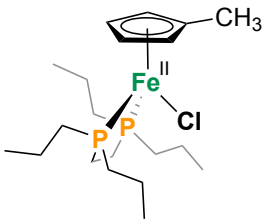

[(η^5-C_5H_4Me)Fe^{II}(d*n*ppe)Cl] (**1**; $C_{20}H_{39}ClFeP_2$, Mw = 432.77 g/mol). In a glovebox, [Fe^{II}(d*n*ppe)$_2Cl_2$] (168.8 mg, 0.259 mmol) was dissolved in THF (2 mL) in a 100 mL bomb. $NaCp^{Me}$ (37.0 mg, 0.363 mmol, 1.4 equiv) was added, and the mixture was stirred at 45 °C for 4 h, yielding a purple-brown solution. The reaction mixture was returned to the glovebox, volatiles were removed in vacuo, and the residue was dissolved in hexanes. Crystals of **1** suitable for X-ray diffraction were obtained by cooling a 1 mL hexane solution in a 4 mL scintillation vial at −35 °C overnight (73 mg, 66%). **^{1}H NMR (400 MHz, C_6D_6, 298 K):** δ_H = 4.59 (s, 2H; η^5-C_5-H), 2.66 (s, 2H; η^5-C_5-H), 2.25 (m, 2H; CH_2), 2.18 (s, 3H; η^5-C_5-CH_3), 2.17 (m, 2H; CH_2), 1.84 (m, 2H; CH_2), 1.57 (m, 4H; CH_2), 1.30 (m, 10H; CH_2), 1.08 (t, $J_{H,H}$ = 8.0 Hz, 6H; P-CH_2-CH_2-CH_3) 0.82 (t, $J_{H,H}$ = 8.0 Hz, 6H; P-CH_2-CH_2-CH_3). **^{31}P{^{1}H} NMR (162 MHz, C_6D_6, 298 K):** δ_P = 89.2. **^{13}C{^{1}H} (101 MHz, C_6D_6, 298 K):** δ_C = 98.4 (t, $J_{C,P}$ = 2.5 Hz, C_5H_4–CH_3), 76.6 (t, $J_{C,P}$ = 4.5 Hz, C_5H_4–CH_3), 63.8 (s, C_5H_4–CH_3), 32.7 (dd, $J_{P,C}$ = 8.0 Hz, 10.9 Hz, CH_2), 27.8 (dd, $J_{P,C}$ = 10.3 Hz, 12.1 Hz, CH_2), 20.1 (app t., $J_{P,C}$ = 20.1 Hz, CH_2), 18.4 (t, $J_{P,C}$ = 2.7 Hz, backbone CH_2), 16.6 (app. t, $J_{P,C}$ = 7.4 Hz, CH_3), 16.4 (app. t, $J_{P,C}$ = 5.0 Hz, CH_3), 13.2 (s, Cp-CH_3). **LIFDI-HRMS:** $C_{20}H_{39}ClFeP_2$ ($[M]^+$) (432.156, calculated); (432.155, observed).

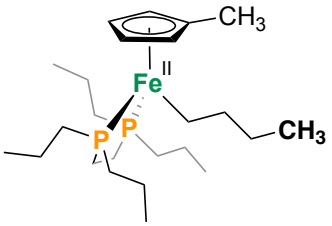

[(η^5-C_5H_4Me)Fe^{II}(d*n*ppe)^{n}Bu] (**2**; $C_{24}H_{48}FeP_2$, Mw = 454.43 g/mol). In a glovebox, **1** (11.0 mg, 0.0254 mmol) was dissolved in THF (2 mL) in a 20 mL scintillation vial, and *n*-BuLi (30.5 µL, 3 equiv., 0.0763 mmol) was added at −35 °C. The reaction was allowed to warm to room temperature over 15 min, affording an orange solution containing **2**, **3**, and **4** in

a 0.15:0.47:0.38 ratio (by ^{31}P NMR spectroscopy). The mixture was stirred for an additional 12 h at 25 °C, filtered, and the solvent removed *in vacuo*, providing a residue in which **2** was the major component. This material was obtained in sufficient purity (>90% by ^{31}P NMR) and quantity (~ 2 mg) for NMR and MS characterization. **^{1}H NMR (400 MHz, C_6D_6, 298 K):** δ_H = 4.12 (s, 2H; η^5-C_5-H), 3.69 (s, 2H; η^5-C_5-H), 1.98 (s, 3H; η^5-C_5-CH_3), 1.80-1.06 (m, 20 H; overlapping CH_2), 1.60 (m, 2H; one of Fe-$CH_2CH_2CH_2CH_3$ determined by ^{1}H 1D-TOCSY), 1.54 (m, 2H; one of Fe-$CH_2CH_2CH_2CH_3$ determined by ^{1}H 1D-TOCSY), 1.18 (t, $J_{H,H}$ = 7.2 Hz, 3H; Fe-$CH_2CH_2CH_2CH_3$), 1.03 (t, $J_{H,H}$ = 7.5 Hz, 6H; P-CH_2-CH_2-CH_3), 0.96 (t, $J_{H,H}$ = 7.4 Hz, 6H; P-CH_2-CH_2-CH_3), -0.24 (m, 2H; Fe-$CH_2CH_2CH_2CH_3$). **^{31}P{^{1}H} NMR (162 MHz, C_6D_6, 298 K):** δ_P = 97.5. **^{13}C{^{1}H} (101 MHz, C_6D_6, 298 K, selected by ^{1}H-^{13}C HSQC):** δ_C = 76.8 (C_5H_4–CH_3), 70.5 (C_5H_4–CH_3), 41.5 (one of Fe-$CH_2CH_2CH_2CH_3$), 30.0 (one of Fe-$CH_2CH_2CH_2CH_3$), 14.3 (Fe-$CH_2CH_2CH_2CH_3$), 12.5 (Cp-CH_3), 3.61 (Fe-$CH_2CH_2CH_2CH_3$). **LIFDI-HRMS:** $C_{24}H_{48}FeP_2$ ([M]$^+$) (454.257, calculated); (454.258, observed).

[(η^5-C_5H_4Me)Fe^{II}(d*n*ppe)H] (**3**; $C_{20}H_{40}FeP_2$, Mw = 398.32 g/mol). In a glovebox, **1** (14.8 mg, 0.0342 mmol) was dissolved in THF (2 mL) in a 20 mL scintillation vial. *t*-BuLi (4.38 mg, 0.0684 mmol, 2.0 equiv) was added at −35 °C, and the mixture was allowed to warm to room temperature over 15 min, affording a yellow solution. Volatiles were removed in vacuo to yield **3** as a yellow solid (10 mg, 74%). **^{1}H NMR (400 MHz, C_6D_6, 298 K):** δ_H = 4.21 (s, 2H; η^5-C_5-H), 4.04 (s, 2H; η^5-C_5-H), 2.13 (s, 3H; η^5-C_5-CH_3)), 1.78-1.03 (m, 20 H; overlapping CH_2), 0.99 (t, $J_{H,H}$ = 7.0 Hz, 6H; P-CH_2-CH_2-CH_3), 0.94 (t, $J_{H,H}$ = 7.3 Hz, 6H; P-CH_2-CH_2-CH_3), -17.3 (t, $J_{P,H}$ = 72.3 Hz, 1H; Fe-H). **^{31}P{^{1}H} NMR (162 MHz, C_6D_6, 298 K):** δ_P = 102.8. **^{13}C{^{1}H} (101 MHz,**

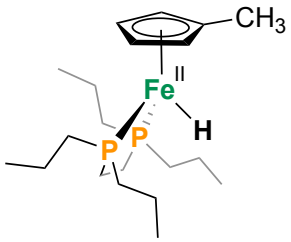

C_6D_6, 298 K): δ_C = 89.3 (t, $J_{C,P}$ = 1.8 Hz, $\underline{C}_5H_4$–CH_3), 73.3 (br. s, $\underline{C}_5H_4$–CH_3), 71.6 (s, $\underline{C}_5H_4$–CH_3), 39.1 (m, $\underline{C}H_2$), 37.0 (m, $\underline{C}H_2$), 27.5 (dd, $J_{P,C}$ = 10.3 Hz, 12.1 Hz, $\underline{C}H_2$), 16.8 (s, Cp-$\underline{C}H_3$), 16.7 (t, $J_{H,P}$ = 5.6 Hz, $\underline{C}H_3$), 16.5 (t, $J_{H,P}$ = 6.7 Hz, $\underline{C}H_3$). **FT-IR (ATR, hexane film):** υ = 1,830 cm^{-1} ([Fe]-H). **LIFDI-HRMS:** $C_{20}H_{40}FeP_2$ ($[M]^+$) (398.195, calculated); (398.195, observed).

[(η^5-C_5H_4Me)Fe^{II}(κ^3-*P,C,P*-d*n*ppe)] (**4**; $C_{20}H_{38}FeP_2$, Mw = 396.31 g/mol). In a glovebox, **1** (21.4 mg, 0.0494 mmol) in a 20 mL scintillation vial was cooled to −78 °C. *n*-BuLi (59.3 µL, 2.5 M in hexanes, 0.0701 mmol, 3.0 equiv) was added at −78 °C, and the mixture was stirred for 30 min. The reaction was then warmed to room temperature over 10 min, affording a deep red solution. Quantitative ^{31}P NMR spectroscopy indicated 90% conversion to **4**.

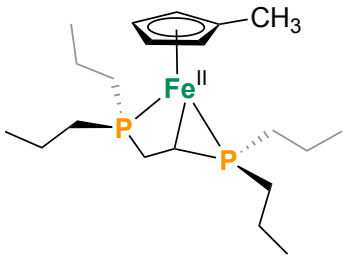

^1H NMR (400 MHz, C_6D_6, 298 K): δ_H = 4.25 (s, 1H; η^5-C_5-$\underline{H}$), 4.14 (s, 1H; η^5-C_5-$\underline{H}$), 3.98 (s, 1H; η^5-C_5-$\underline{H}$), 3.82 (s, 1H; η^5-C_5-$\underline{H}$), 2.82 (m, 1H; P-C$\underline{H}_2$-CH-P, see MS for fitting parameters), 2.23-1.08 (m, 16H; C$\underline{H}_2$), 2.17 (m, 1H; P-C$\underline{H}_2$-CH-P, see MS for fitting parameters), 2.08 (s, 3H; η^5-C_5-C$\underline{H}_3$), 1.08-0.89 (m, 12H; overlapping P-C$\underline{H}_2$-CH_2-CH_3), -0.14 (m, 1H; P-CH_2-C$\underline{H}$-P, see MS for fitting parameters). **$^{31}P\{^1H\}$ NMR (162 MHz, C_6D_6, 298 K):** δ_P = 1.65 (d, $J_{P,P}$ = 32.2 Hz), -1.22 (d, $J_{P,P}$ = 32.2 Hz). **$^{13}C\{^1H\}$ (101 MHz, C_6D_6, 298 K, selected by ^1H-^{13}C HSQC):** δ_C = 69.7 ($\underline{C}_5H_4$–CH_3), 69.2 ($\underline{C}_5H_4$–CH_3), 69.0 ($\underline{C}_5H_4$–CH_3), 67.0 ($\underline{C}_5H_4$–CH_3), 36.0 (P-$\underline{C}H_2$-CH-P), 15.6 (s, Cp-$\underline{C}H_3$), -25.1 (P-CH_2-$\underline{C}$H-P). **LIFDI-MS:** $C_{20}H_{38}FeP_2$ ($[M]^+$) (396.180, calculated); (396.179, observed) & $C_{20}H_{39}FeP_2$ ($[M+H]^+$) (397.187, calculated); (397.187, observed) in a 2:3 ratio.

[(η^5-C_5H_4Me)Fe^{II}(d*n*ppe)N_2][BPh_4] (**5**; $C_{44}H_{59}N_2FeP_2B$, Mw = 744.55 g/mol). In a glovebox, **1** (19.5 mg, 0.0451 mmol) was dissolved in Et_2O (2 mL) in a 20 mL scintillation vial. $NaBPh_4$ (14.8 mg, 0.0428 mmol, 0.95 equiv) was added, and the mixture was stirred to afford a cloudy, opaque yellow solution. The reaction mixture was filtered through Celite®, and volatiles were removed in vacuo to yield **5** as a yellow solid (22 mg, 66%). **^{1}H NMR (400 MHz, THF-d_8, 298 K):** δ_H = 7.27 (br, 8H; *o*-$BC_6\underline{H}_5$), 6.85 (t, $J_{H,H}$ = 7.1 Hz, 8H; *m*-$BC_6\underline{H}_5$), 6.70 (t, $J_{H,H}$ = 7.1 Hz, 4H; *p*-$BC_6\underline{H}_5$), 4.86 (s, 2H; η^5-C_5-$\underline{H}$), 3.93 (s, 2H; η^5-C_5-$\underline{H}$), 2.04 (m, 2H; $C\underline{H}_2$), 1.93 (m, 2H; $C\underline{H}_2$), 1.88 (s, 3H; η^5-C_5-$C\underline{H}_3$), 1.84-1.40 (m, 16H; overlapping $C\underline{H}_2$), 1.09 (t, $J_{H,H}$ = 7.0 Hz, 6H; P-CH_2-CH_2-$C\underline{H}_3$) 1.03 (t, $J_{H,H}$ = 7.2 Hz, 6H; P-CH_2-CH_2-$C\underline{H}_3$). **^{31}P{^{1}H} NMR (162 MHz, THF-d_8, 298 K):** δ_P = 83.6. **^{13}C{^{1}H} (101 MHz, THF-d_8, 298 K):** δ_C = 165.1 (q, $J_{B,C}$ = 49.8 Hz, B-$\underline{C}$(ipso)), 137.0 (s, *o*-$B\underline{C}_6H_5$), 125.5 (m, *m*-$B\underline{C}_6H_5$), 121.6 (s, *p*-$B\underline{C}_6H_5$), 101.7 (t, $J_{C,P}$ = 1.5 Hz, $\underline{C}_5H_4$–CH_3), 82.5 (s, $\underline{C}_5H_4$–CH_3), 76.5 (s, $\underline{C}_5H_4$–CH_3), 68.0 (s, $\underline{C}_5H_4$–CH_3), 30.5 (m, $\underline{C}H_2$), 28.1 (m, $\underline{C}H_2$), 24.6 (app t., $J_{P,C}$ = 21.4 Hz, $\underline{C}H_2$), 18.0 (t, $J_{P,C}$ = 3.4 Hz, backbone $\underline{C}H_2$), 16.0 (app. t, $J_{P,C}$ = 7.7 Hz, $\underline{C}H_3$), 16.4 (app. t, $J_{P,C}$ = 6.2 Hz, $\underline{C}H_3$), 12.1 (s, Cp-$\underline{C}H_3$). **FT-IR (ATR, THF film):** υ = 2,111 cm^{-1} ([Fe]-N≡N). **ESI-HRMS:** $C_{20}H_{39}FeP_2$ ([M-N_2]$^+$) (397.187, calculated); (397.187, observed).

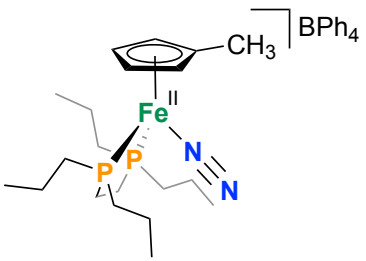

[(η^5-$C_5H_4^{Me}$)Fe^{II}(d*n*ppe))$_2$(μ-dnppe)][BPh_4]$_2$ (**6**; $C_{102}H_{150}Fe_2P_6B_2$, M_W = 1695.43 g/mol). In a 20 mL scintillation vial, **1** (49.7 mg, 0.115 mmol), containing excess free dnppe, was dissolved in Et_2O (2 mL). $NaBPh_4$ (37.3 mg, 0.109 mmol, 0.95 equiv) was added, and the mixture was stirred to afford a cloudy, opaque yellow solution. The resulting yellow solid was dissolved in THF and filtered

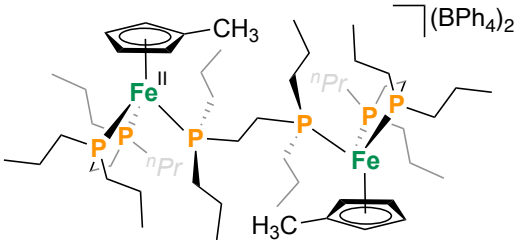

through Celite®; removal of volatiles in vacuo yielded **6** as a yellow solid (82 mg, 85%). Crystals suitable for X-ray diffraction were obtained by layering a THF solution with hexanes in a 4 mL scintillation vial.**^{31}P{^{1}H} NMR (162 MHz, THF-H$_8$, 298 K):** δ_P = 83.1 (d, $J_{P,P}$ = 47.2 Hz, 4P; κ^2-P), 43.3 (t, $J_{P,P}$ = 47.2 Hz, 2P; μ-P). **ESI-HRMS:** $C_{34}H_{71}FeOP_4$ ([M – Cp^{Me}Fe(Dnppe)+ O]$^+$) (675.381, calculated); (675.379, observed). ("O" refers to oxidized phosphine arm).

Reactivity of [Cp*Fe(d*n*ppe)Cl] with *n*-BuLi:

At 195 K: [Cp*Fe(d*n*ppe)Cl] (6.9 mg, 0.0141 mmol) was treated with *n*-BuLi (16.9 μL, 2.5 M in hexanes, 0.0424 mmol, 3.0 equiv) at −78 °C in THF. A ^{31}P{^{1}H} NMR spectrum was acquired using Ph_3P=O (1.2 mg) as an internal standard. Determined yields were: Fe–tucked-in, 43.7%; [Cp(κ^3-P,C,P-dnppe)Fe], 33.0% (**Figure 27**).

At 298 K: [Cp*FeCl(d*n*ppe)] (8.5 mg, 0.0174 mmol) was treated with *n*-BuLi (21 μL, 2.5 M in hexanes, 0.0523 mmol, 3.0 equiv) at 25 °C in THF. A ^{31}P{^{1}H} NMR spectrum was acquired using Ph_3P=O (2.7 mg) as an internal standard. Determined yields were: Fe–tucked-in, 32.3%; [Cp*(d*n*ppe)[Fe]–*n*-Bu], 17.3%; [Cp*(κ^3-P,C,P-d*n*ppe)Fe], 13.4%; and free d*n*ppe, 19.5%. Unlike in the case of Cp^{Me}, Paramagnetic species were also observed by ^{1}H NMR spectroscopy (**Figures S28** and **S29**).

Reactivity of [Cp^{Me}Fe(d*n*ppe)Cl] (1) with *n*-BuLi at 298K:

At 298 K: 1 (5.3 mg, 0.0122 mmol) was treated with *n*-BuLi (13 μL, 2.5 M in hexanes, 0.0367 mmol, 3.0 equiv) at 25 °C in THF. A ^{31}P{^{1}H} NMR spectrum was acquired using Ph_3P=O (2.7 mg) as an internal standard. Determined yields were: [Fe]–H (**3**), 24.2%; [Fe]–*n*-Bu (**2**), 24.2%; and **4**, 3.1% (**Figure S30**).

3. Multinuclear NMR and FT-IR Spectroscopic Data

Figure S1: 1, ^{1}H NMR, C_6D_6, 400 MHz, 298 K.

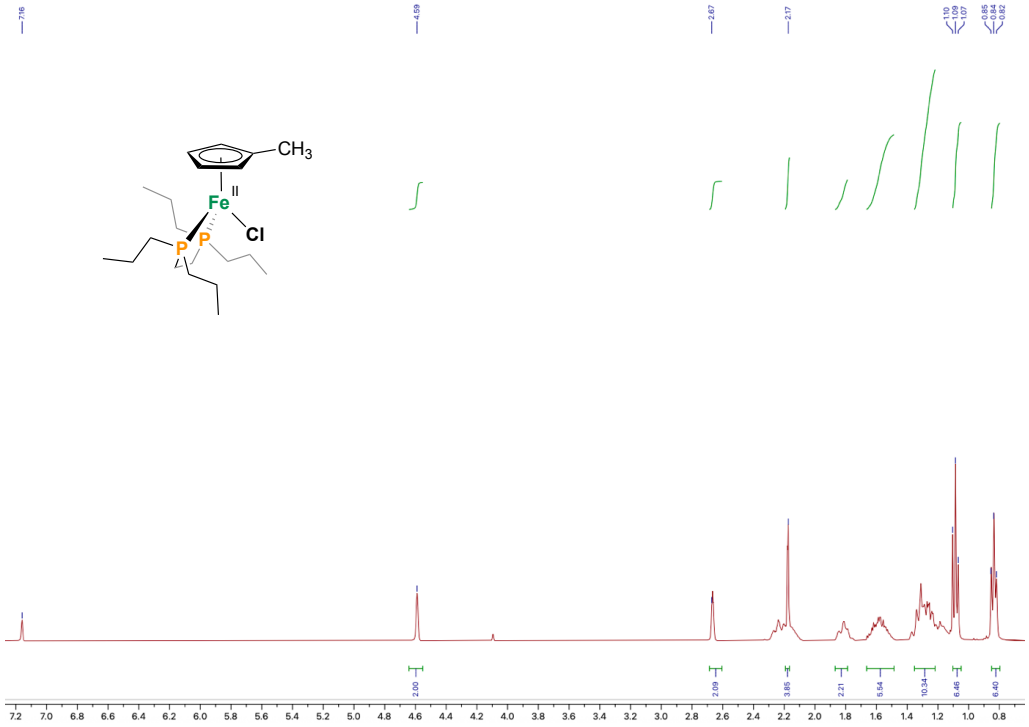

Figure S2: 1, $^{31}P\{^{1}H\}$ NMR, C_6D_6, 162 MHz, 298 K.

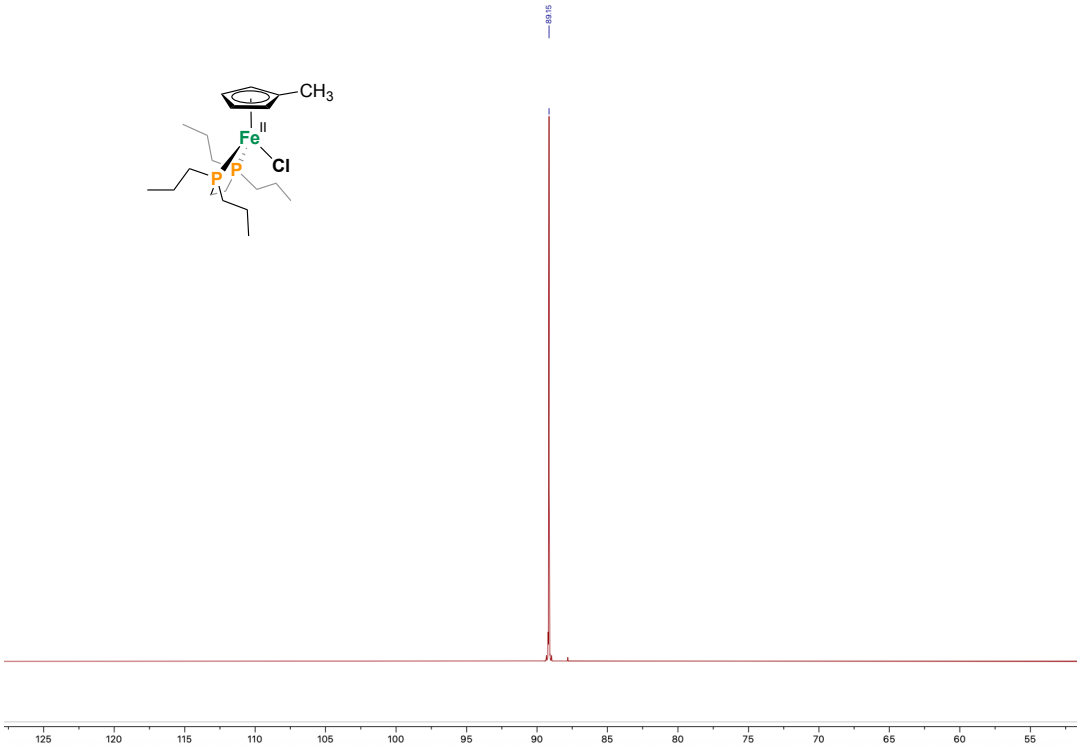

Figure S3: 1, ^{1}H-^{1}H COSY, C_6D_6, 600 MHz, 298 K. Displaying correlation between Cp-H proton signals.

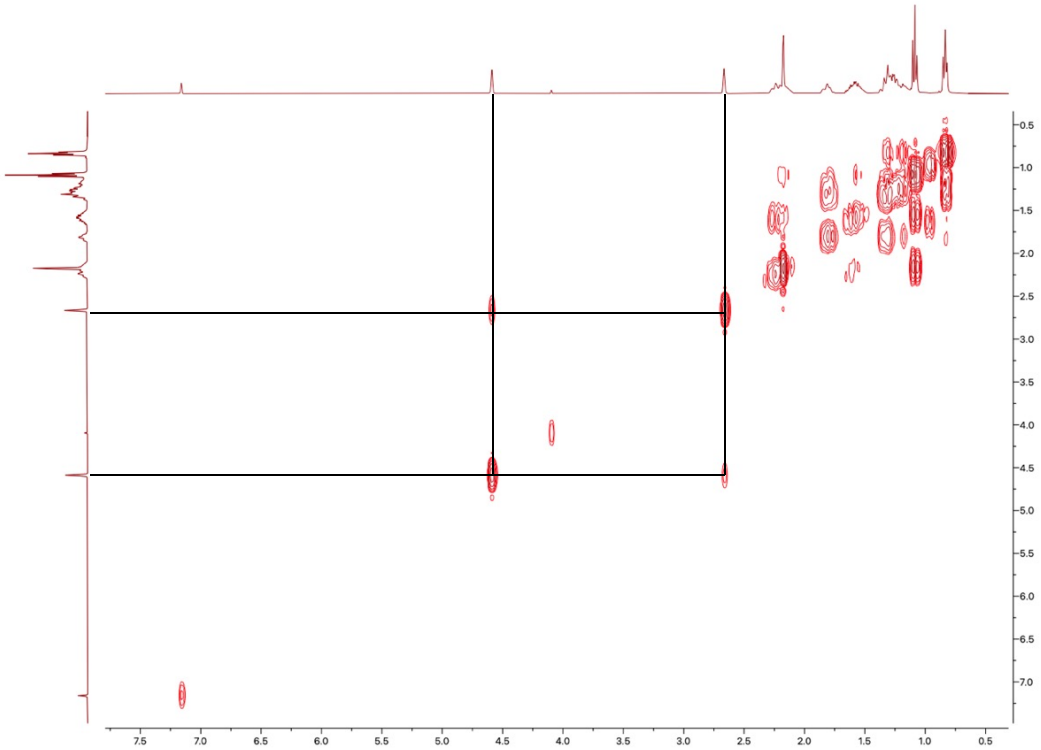

Figure S4: 1, ^{13}C{^{1}H} NMR, C_6D_6, 150.9 MHz, 298 K.

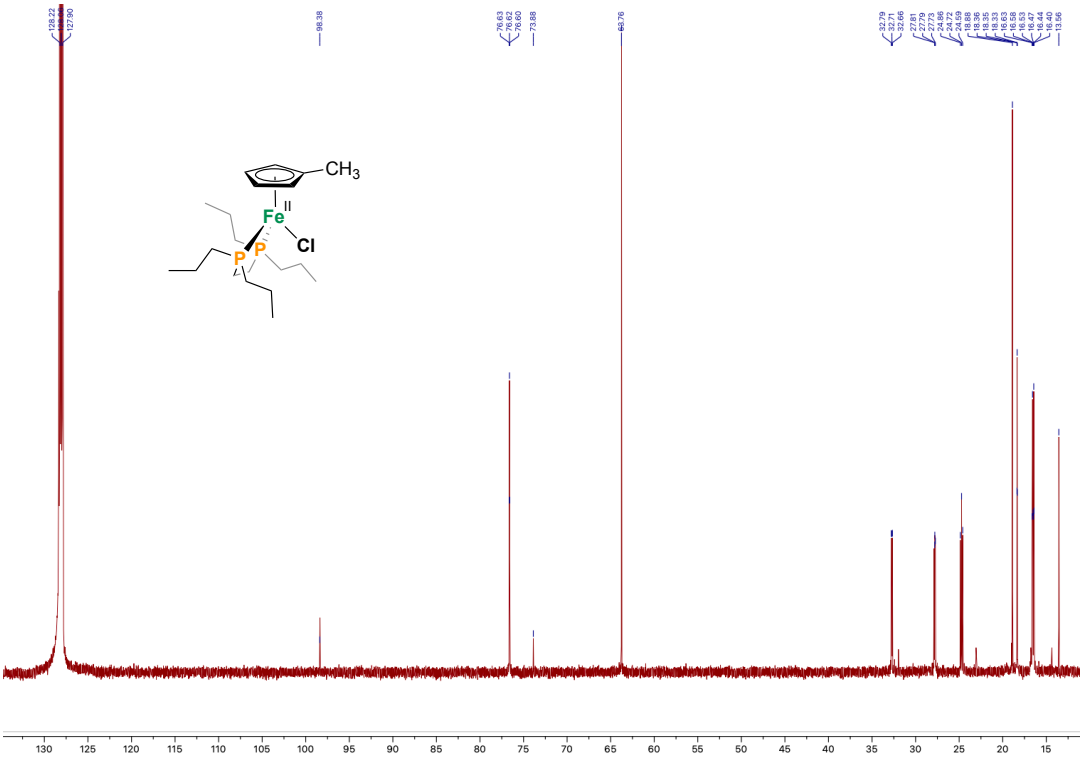

Figure S5: 2, ^{1}H NMR, C_6D_6, 400 MHz, 298 K.

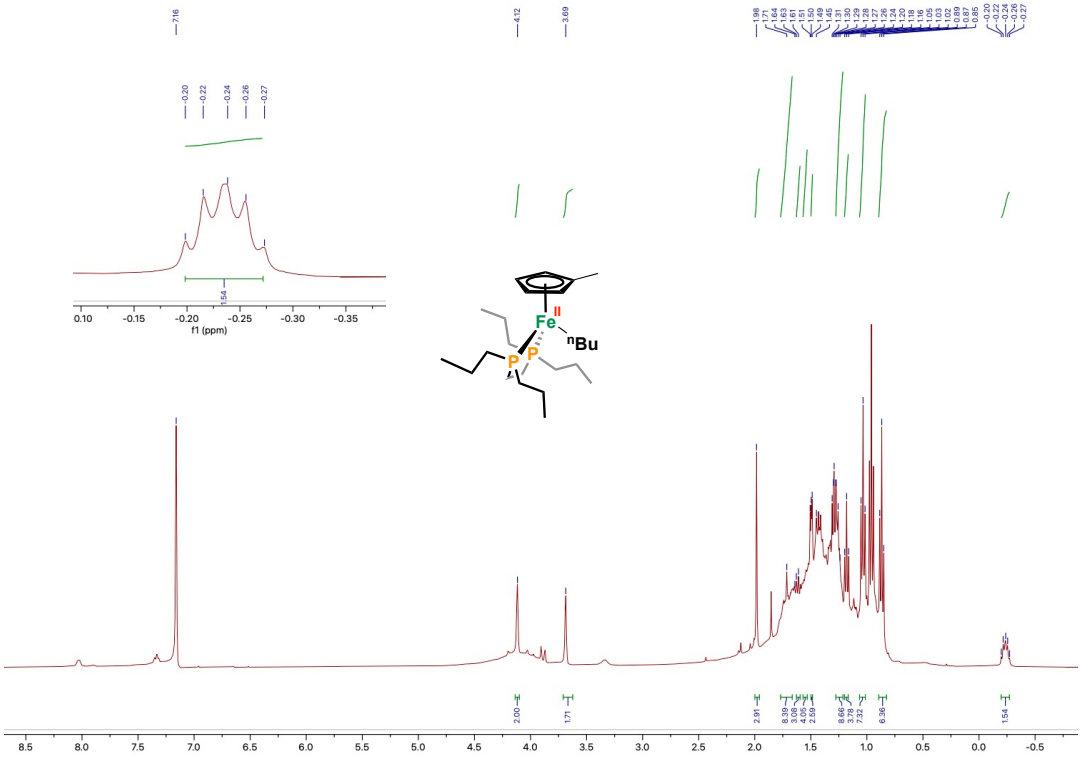

Figure S6: 2, $^{31}P\{^{1}H\}$ NMR, C_6D_6, 162 MHz, 298 K.

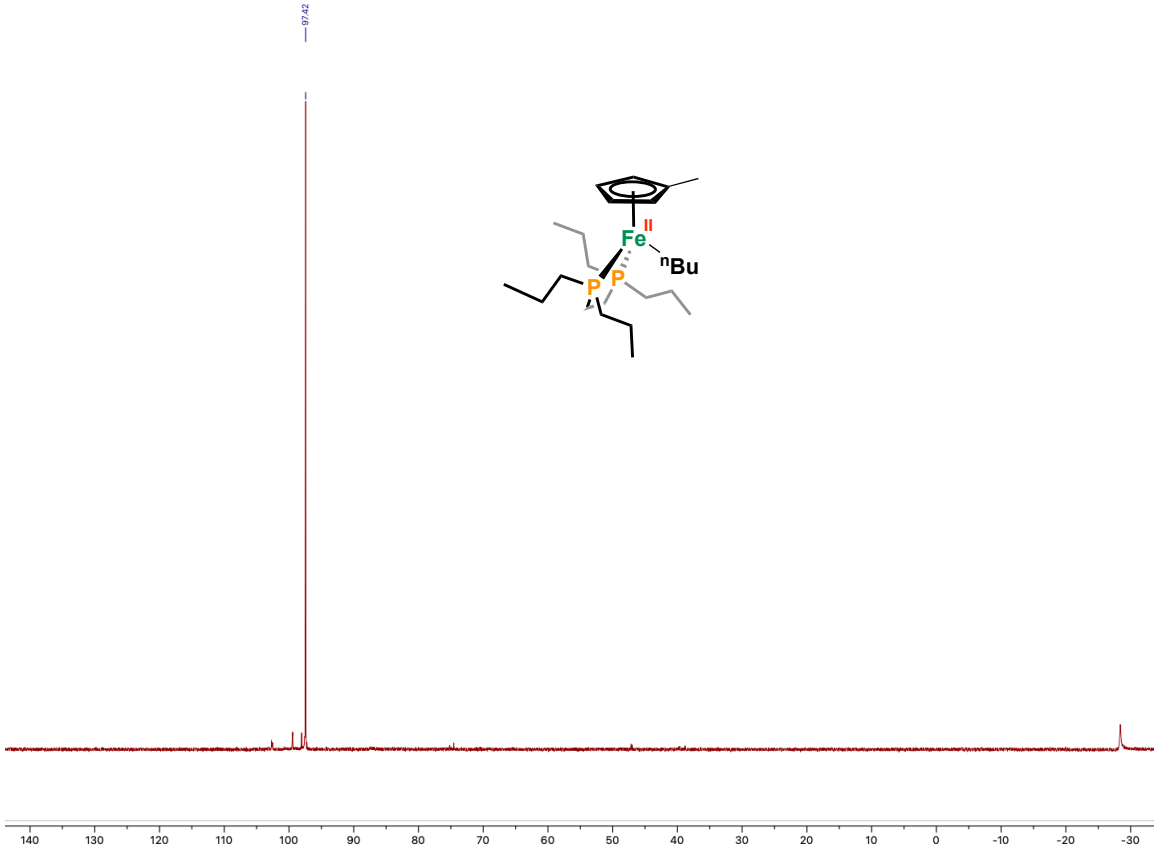

Figure S7: 2, ^{1}H-^{13}C HSQC, C_6D_6, 600 MHz, 298 K. Displays η^5-C_5H_4 and Fe-CH_2 groups.

Figure S8: 2, ^{1}H-^{31}P HMBC, C_6D_6, 600 MHz, 298 K.

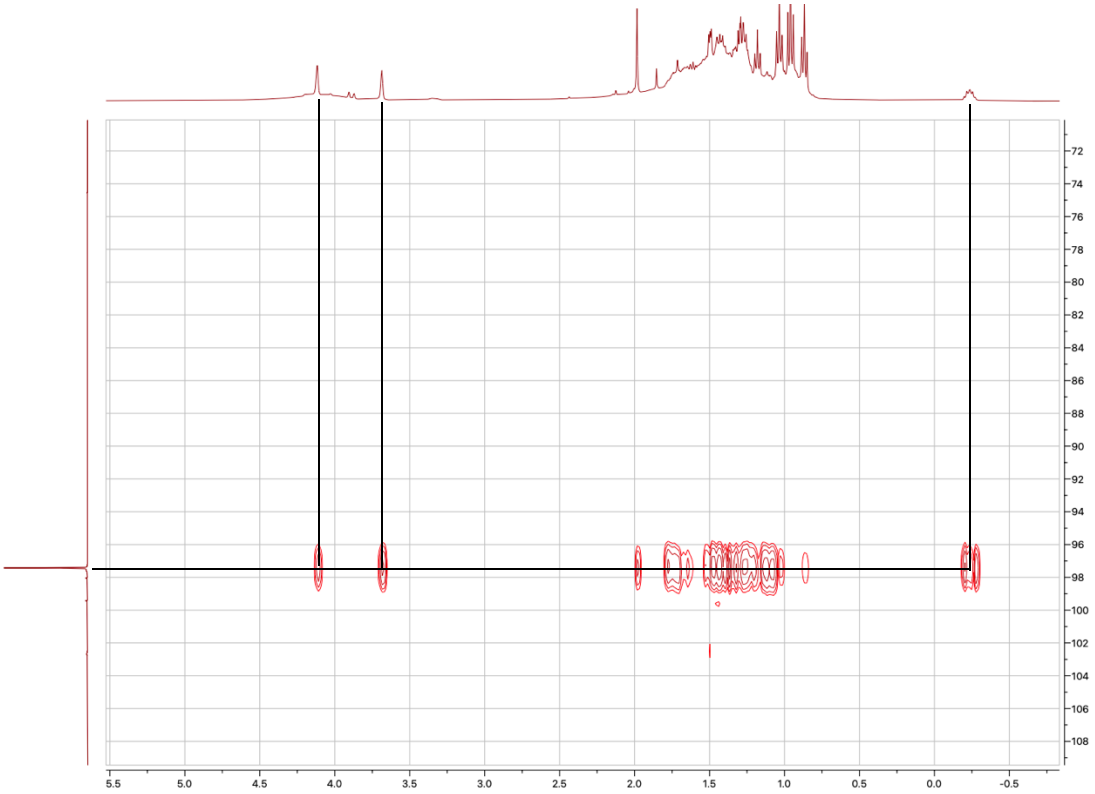

Figure S9: 2, ^{1}H 1D TOCSY, C_6D_6, 600 MHz, 298 K. Displays *n*Bu spin system irradiating peak at -0.25 ppm.

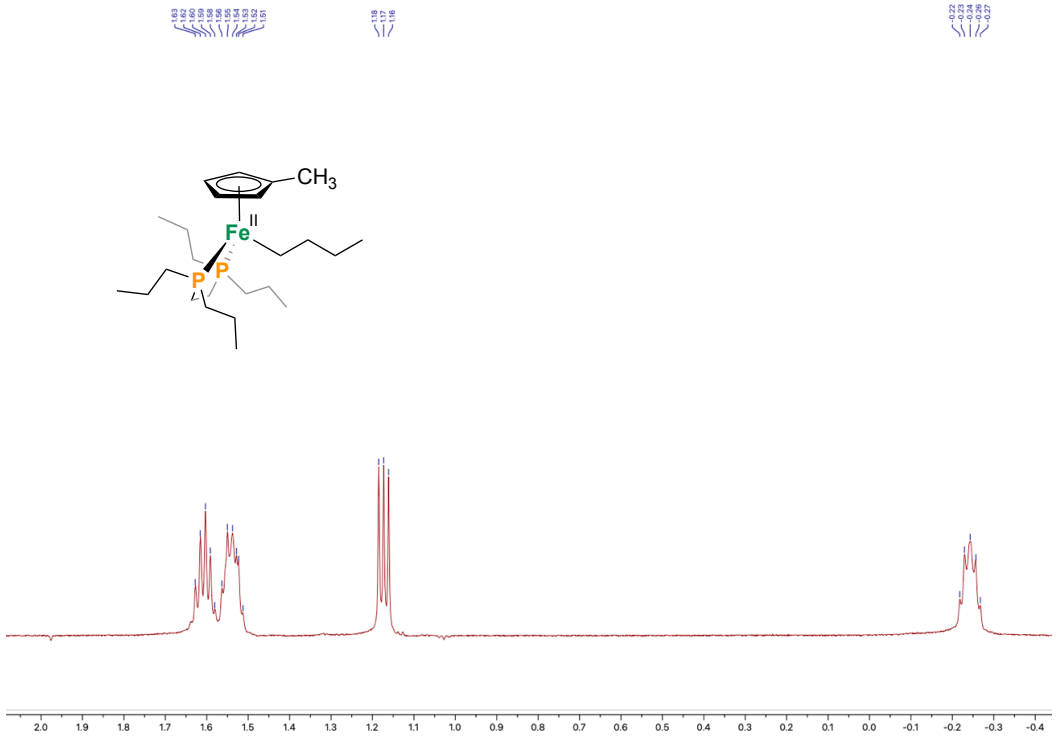

Figure S10: 3, ^{1}H NMR, C_6D_6, 400 MHz, 298 K. Inset shows hydride region. *Unknown impurity

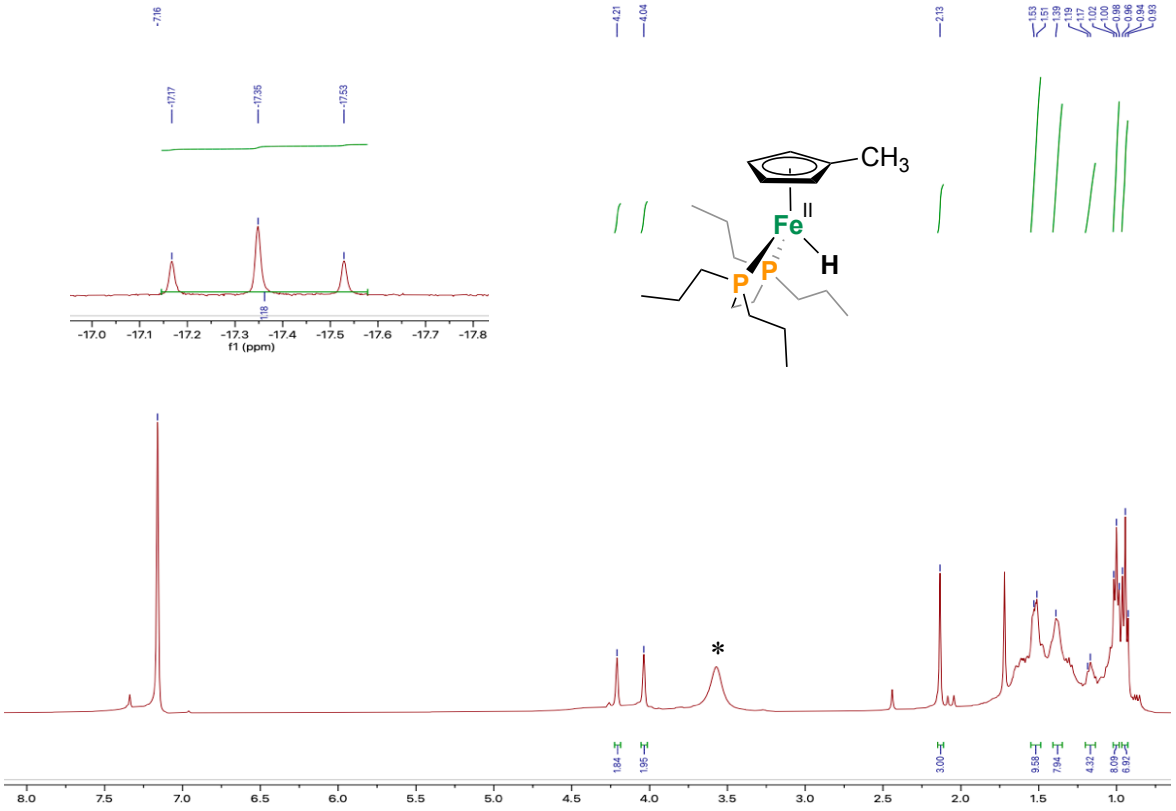

Figure S11: 3, $^{31}P\{^{1}H\}$ NMR, C_6D_6, 162 MHz, 298 K.

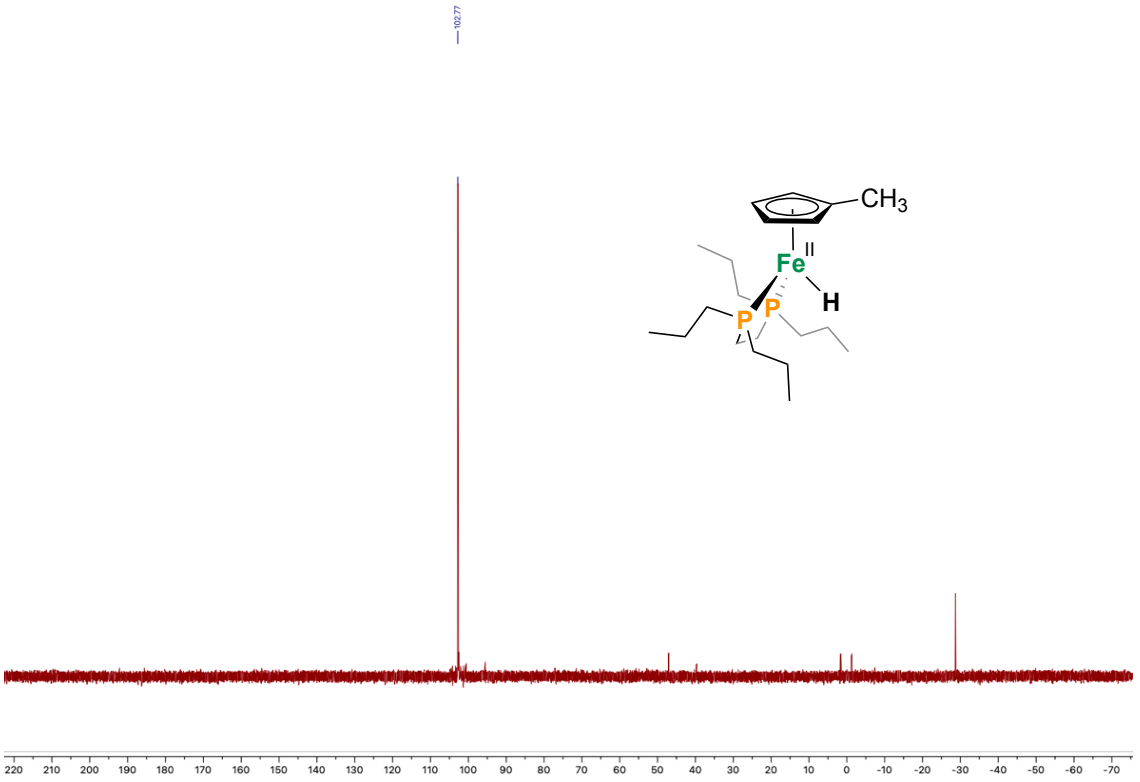

Figure S12: 3, $^{13}C\{^{1}H\}$ NMR, C_6D_6, 150.9 MHz, 298 K.

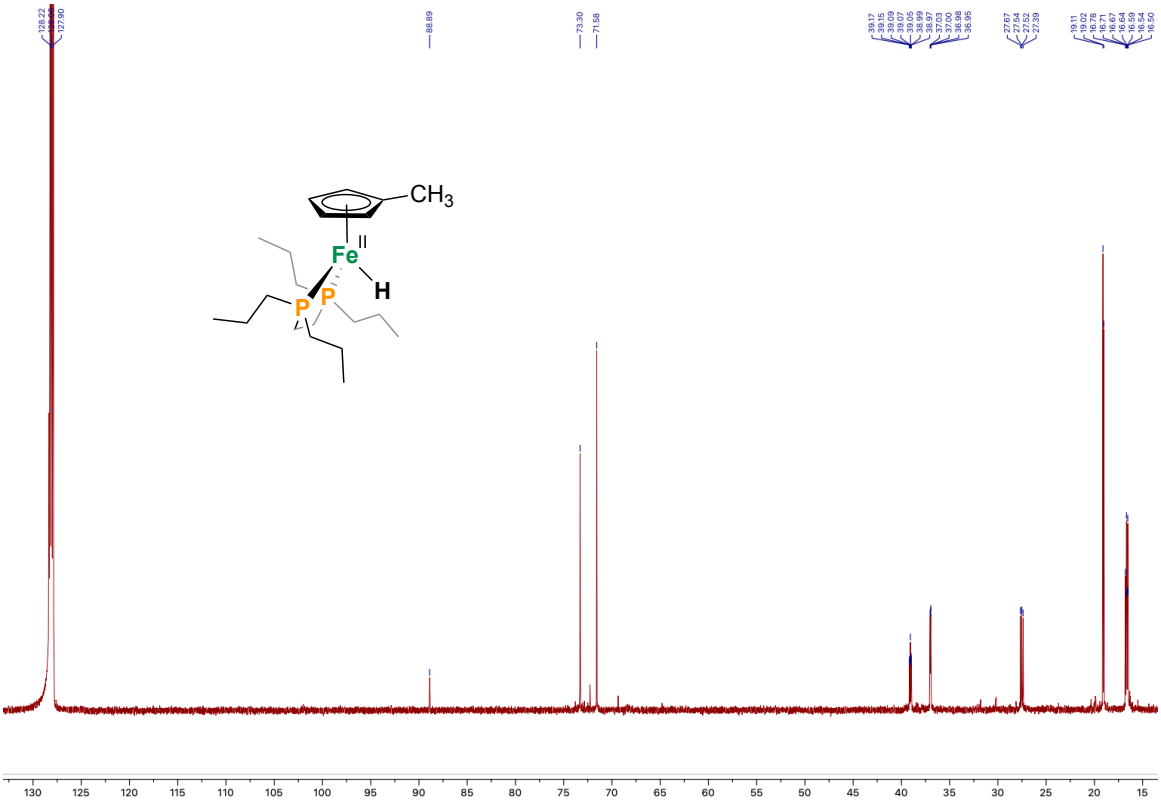

Figure S13: 3, ^{1}H-^{31}P HMBC NMR, C_6D_6, 600 MHz, 298 K. Demonstrating Fe-H and Cp-H signals are consistent with the same molecule.

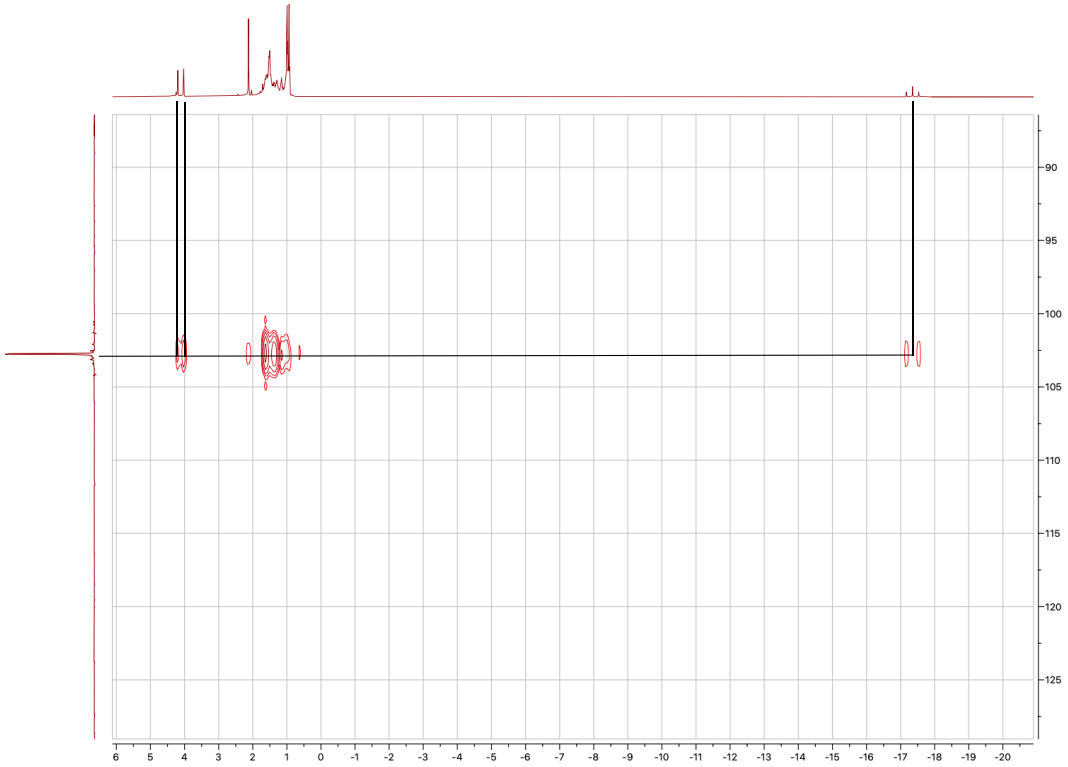

Figure S14: 3 hexane film, FT-IR(ATR), 298K (ν[Fe-H] = 1830 cm^{-1}).

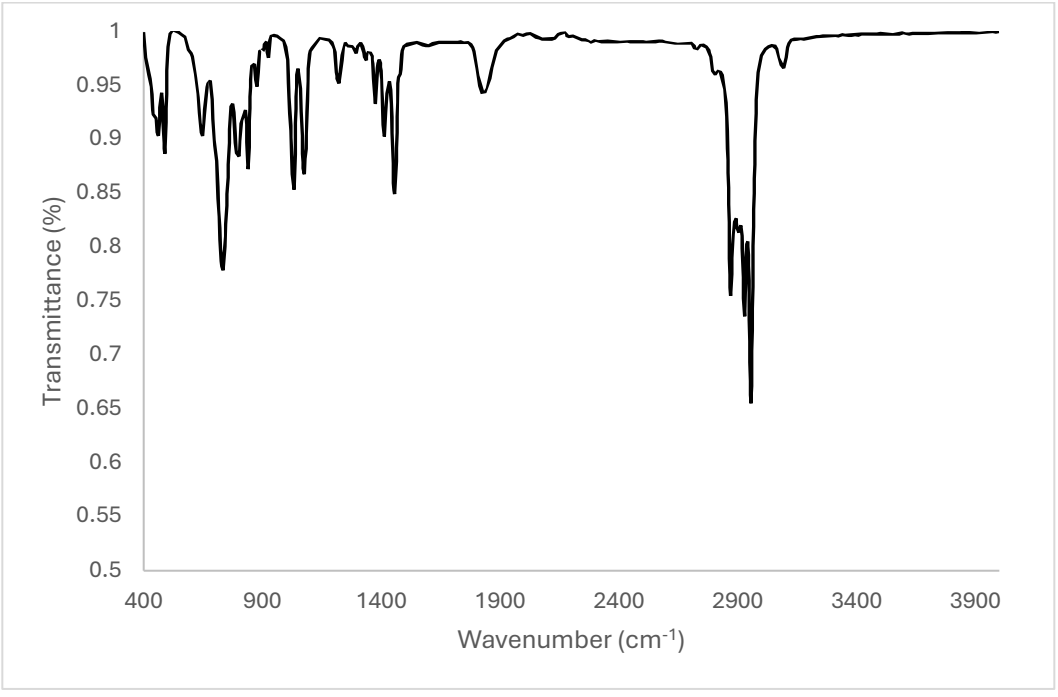

Figure S15: 4, ^{1}H NMR, C_6D_6, 400 MHz, 298 K. *THF impurity

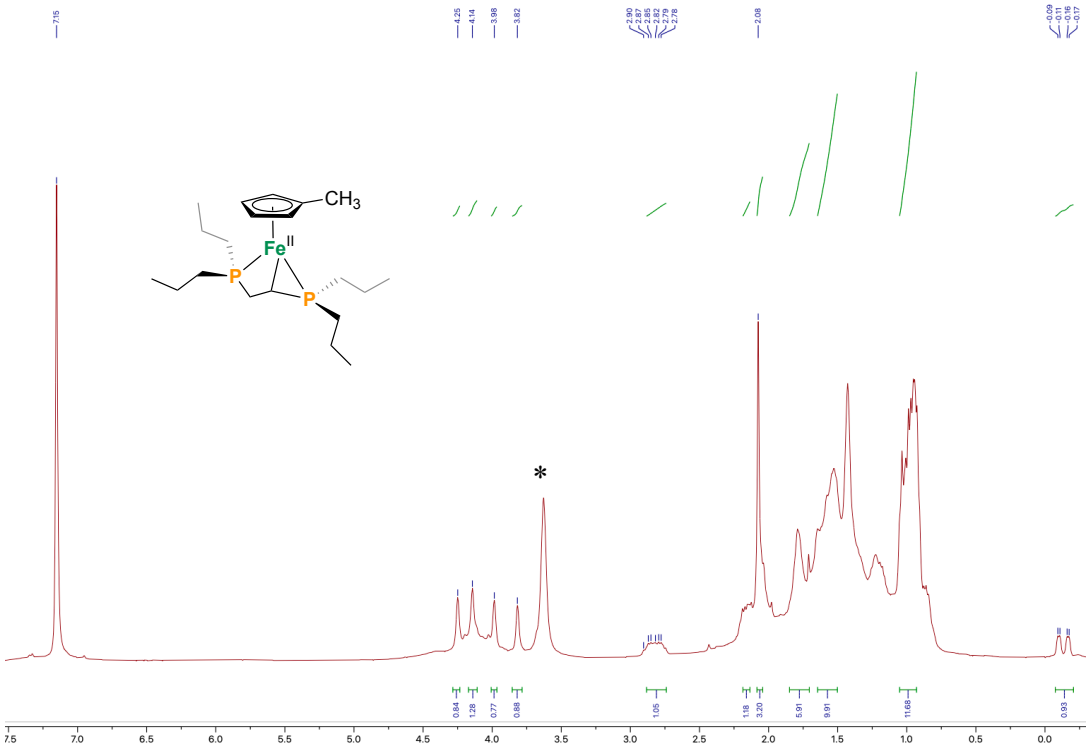

Figure S16: 4, $^{31}P\{^{1}H\}$ NMR, C_6D_6, 162 MHz, 298 K.

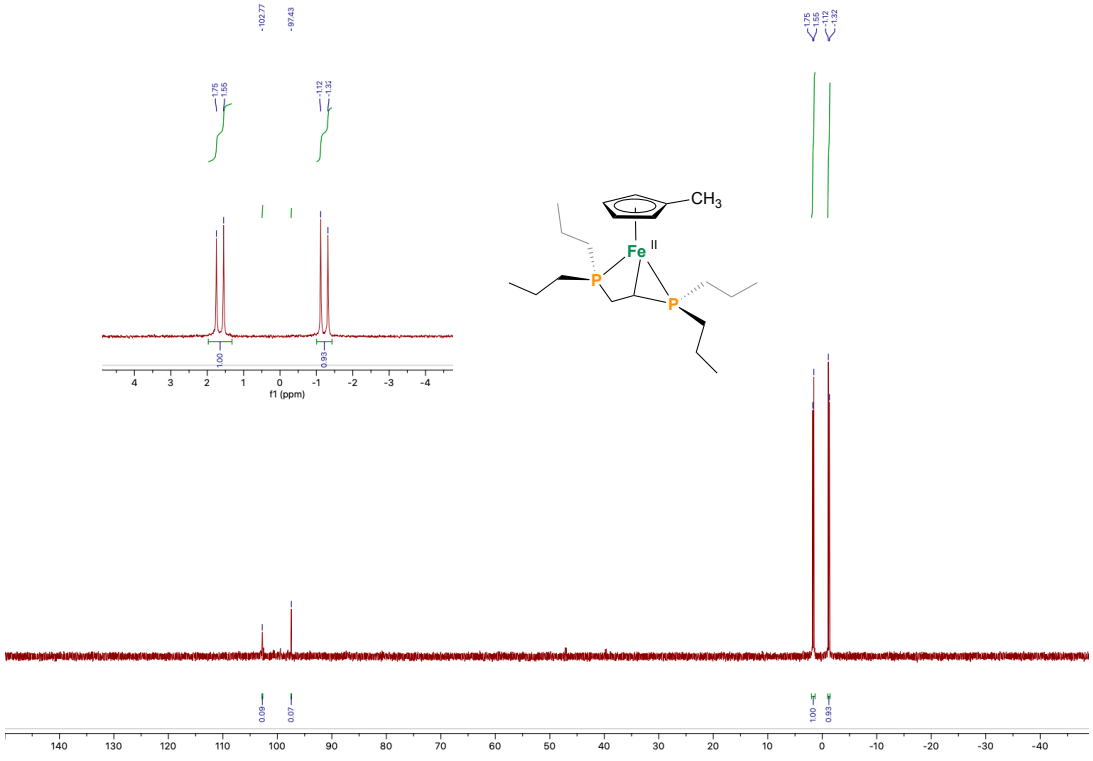

Figure S17: 4, ^{1}H-^{31}P HMBC NMR, C_6D_6, 600 MHz, 298 K. Displaying C_1-symmetry of generated compound via inequivalent Cp-H signals.

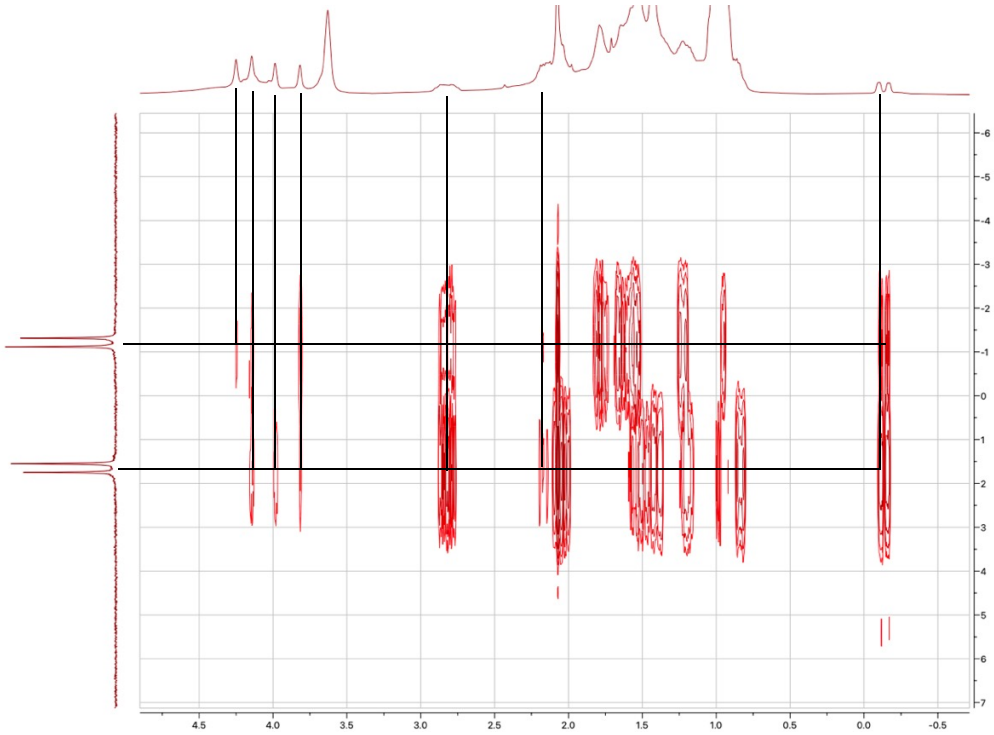

Figure S18: 4, ^{1}H-^{1}H COSY NMR, C_6D_6, 600 MHz, 298 K. Displaying correlation of phosphine coupled proton signals, indicative of the phosphine backbone protons.

Figure S19: 4, ^{1}H-^{13}C HSQC NMR, C_6D_6, 600 MHz, 298 K. Displaying C_1-symmetric nature of complex and the significant upfield shift of the Fe-C signal.

Figure S20: 4, 1D ^{1}H TOCSY NMR, C_6D_6, 600 MHz, 298 K. Displaying Cp^{Me} spin system; ; signal at δ_H = 3.82 ppm was irradiated.

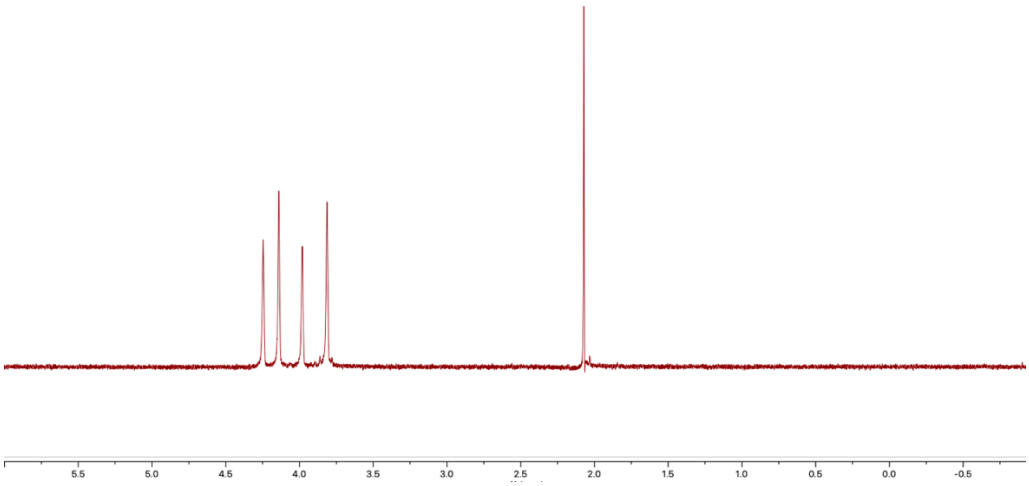

Figure S21: 4, 1D ^{1}H TOCSY NMR, C_6D_6, 600 MHz, 298 K. Displaying PCP backbone spin system; signal at δ_H = -0.2 ppm was irradiated.

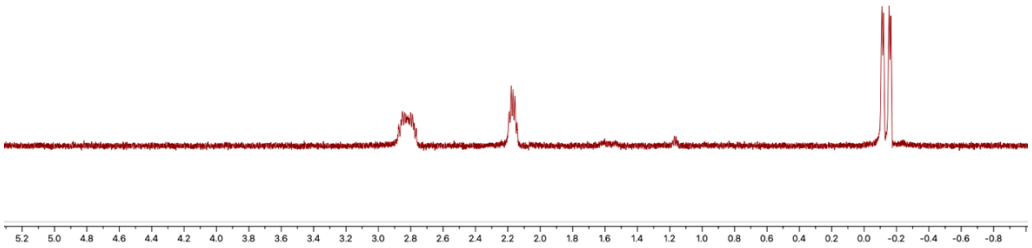

Figure S22: 5, ^{1}H NMR, THF-d_8, 400 MHz, 298 K.

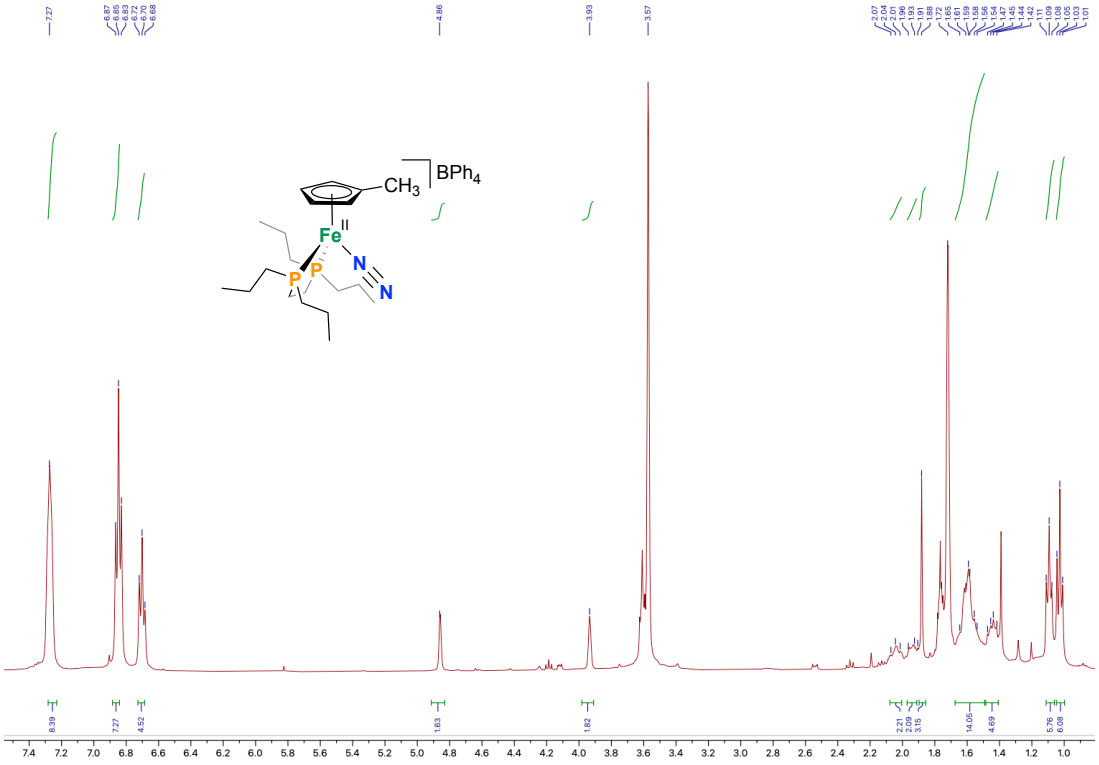

Figure S23: 5, $^{31}P\{^{1}H\}$ NMR, THF-d_8, 162 MHz, 298 K.

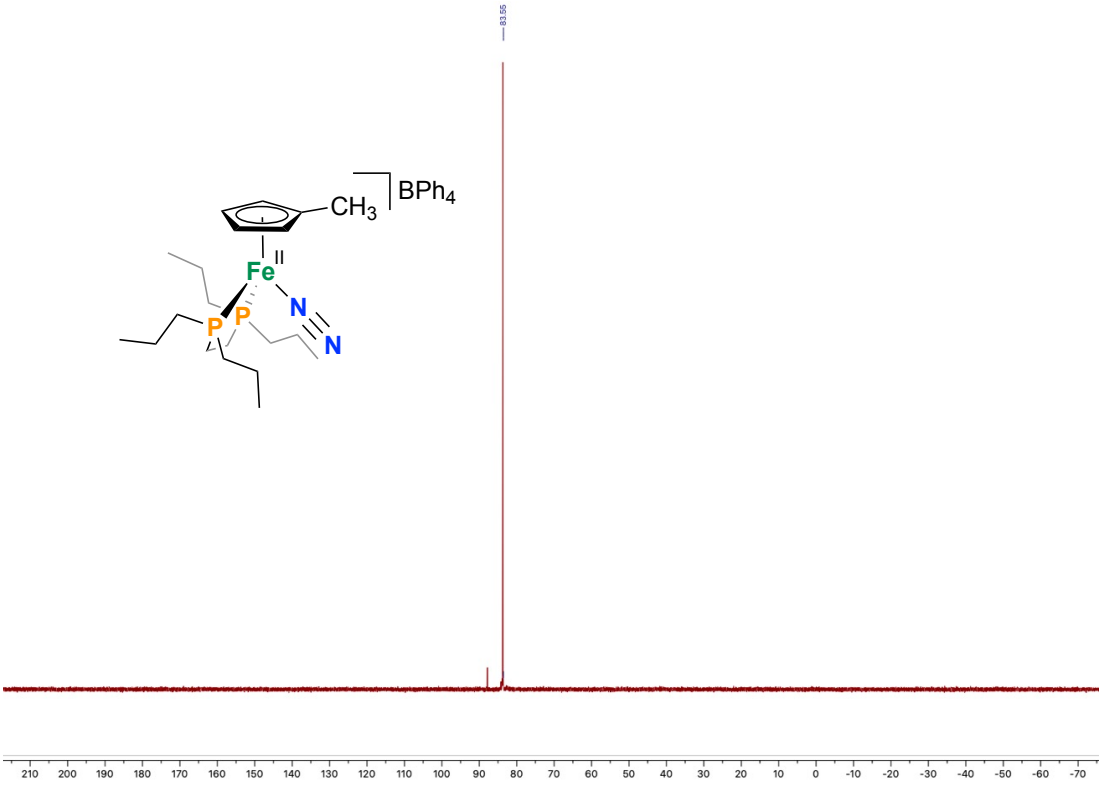

Figure S24: 5, $^{13}C\{^{1}H\}$ NMR, THF-d_8, 150.9 MHz, 298 K.

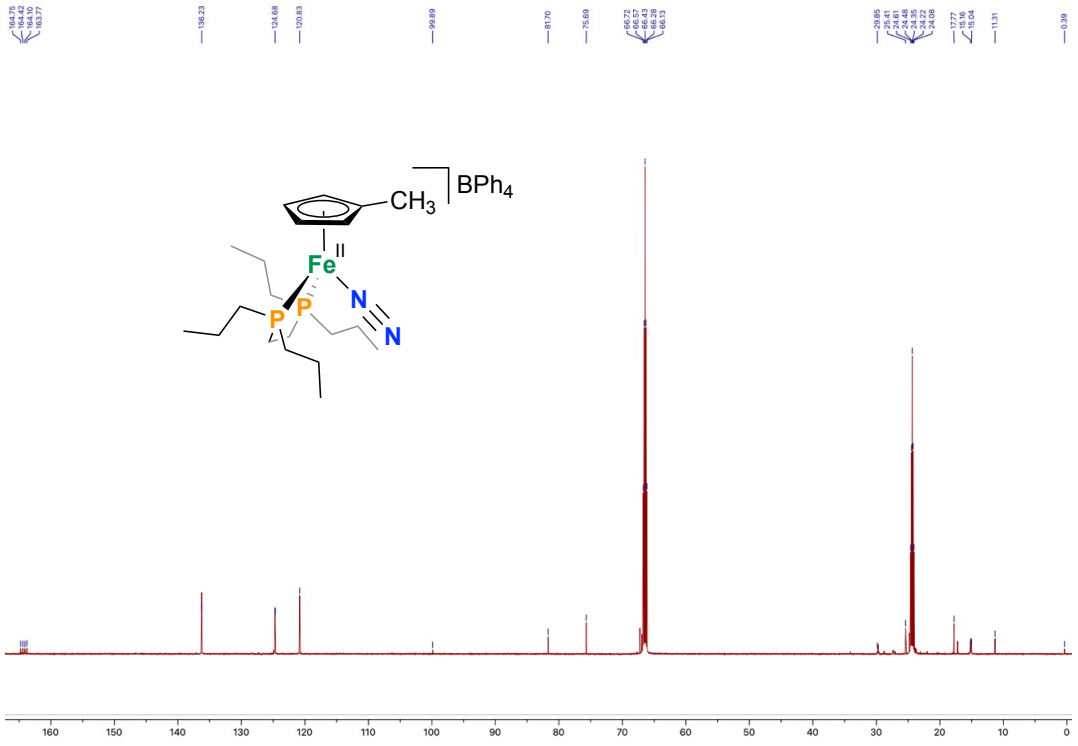

Figure S25: 5, THF film, FT-IR(ATR), 298K (ν[Fe-N≡N] = 2,111 cm^{-1}).

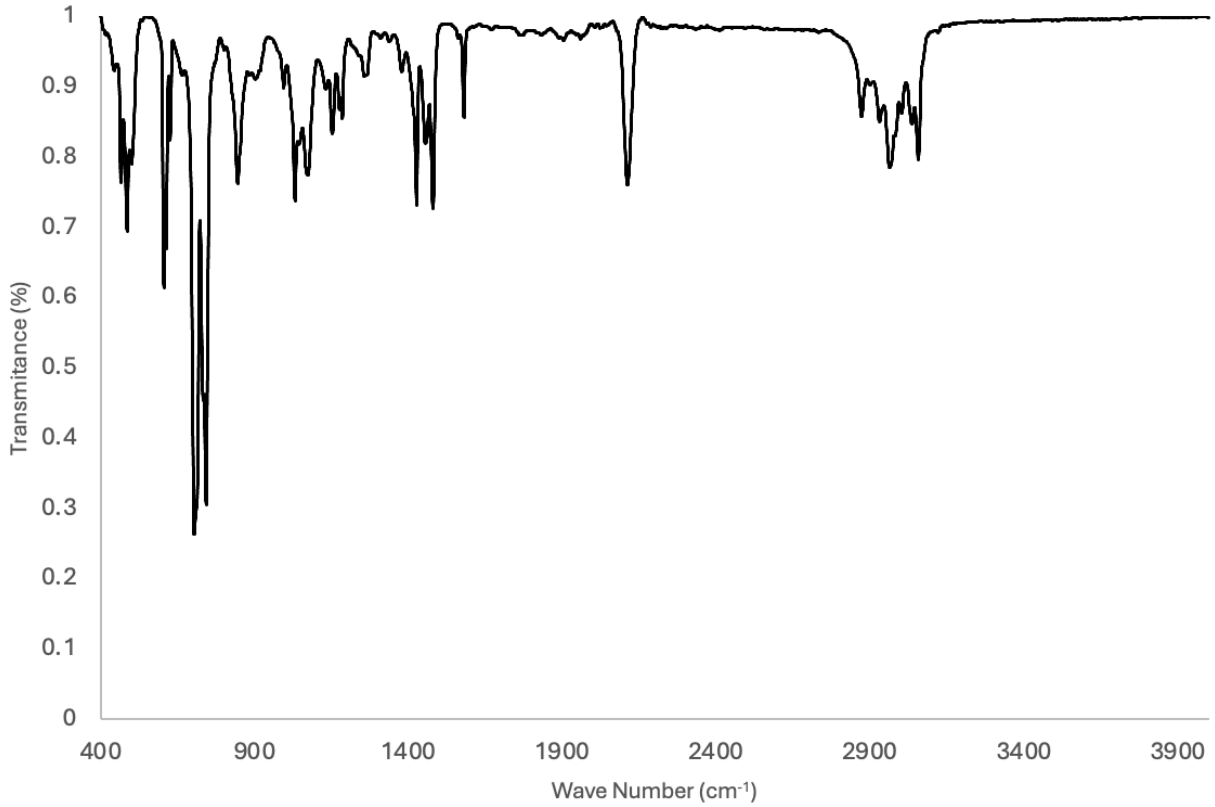

Figure S26: 6, $^{31}P\{^{1}H\}$ NMR, THF-H_8, 162 MHz, 298 K.

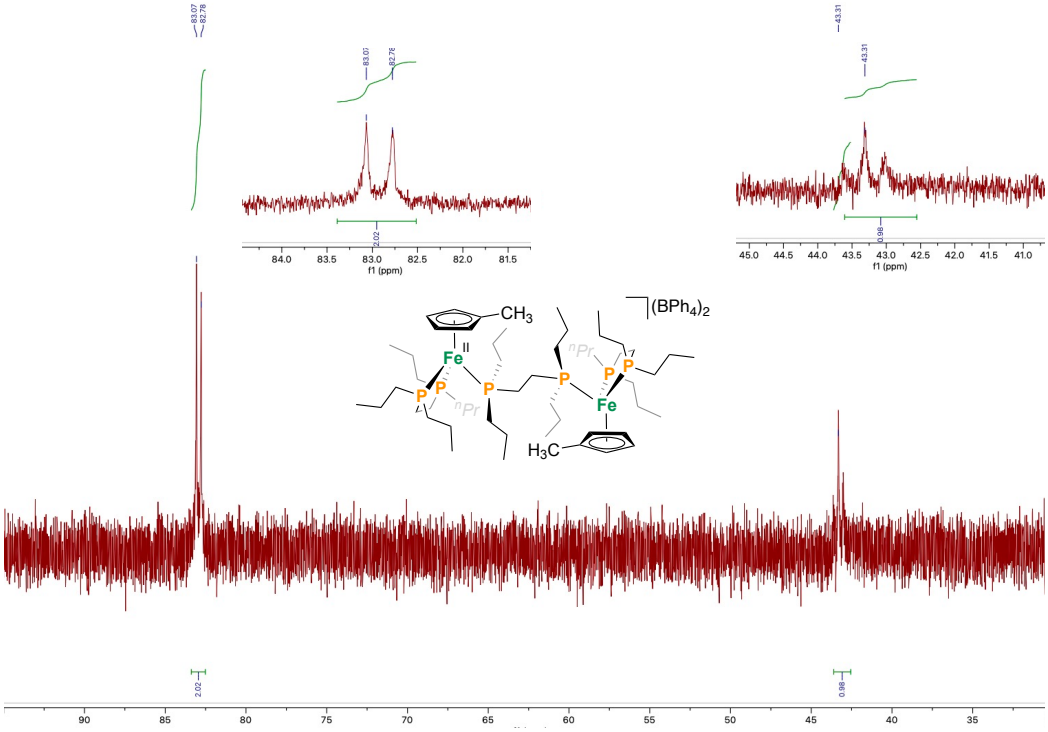

FeCp* and FeCp^{Me} comparison NMR Spectroscopic Data

Figure S27: $^{31}P\{^{1}H\}$ NMR (C_6D_6, 162 MHz, 298 K) of reactivity of [Cp*Fe(d*n*ppe)Cl] with *n*BuLi at -78 °C with a $Ph_3P{=}O$ standard. *Free ligand was present in the starting material.

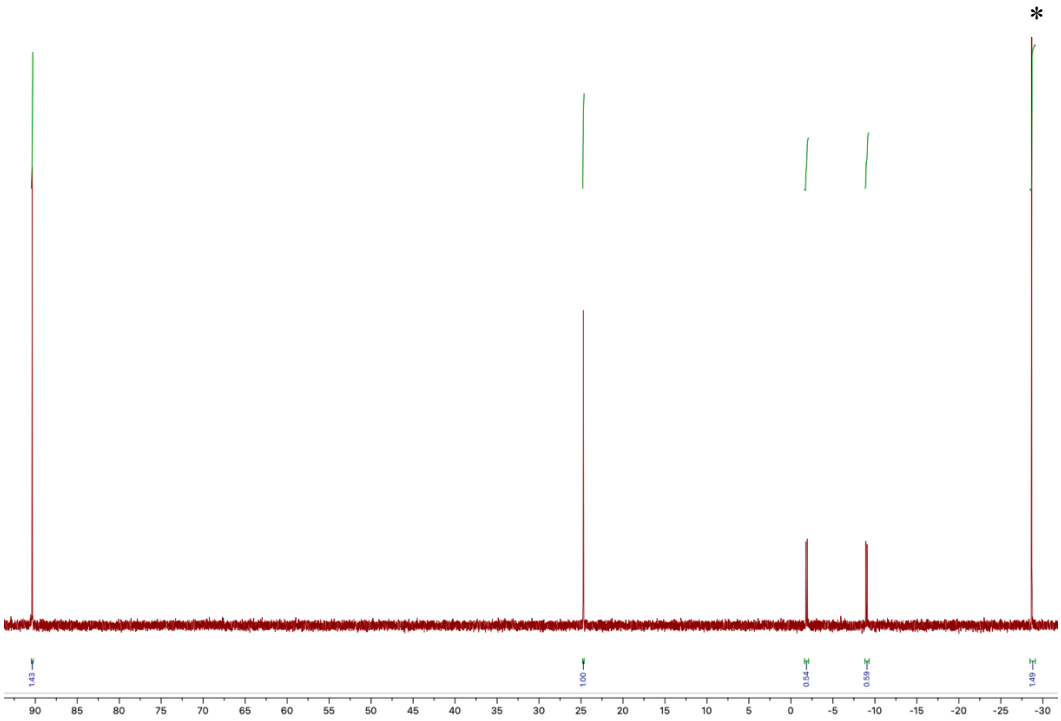

Figure S28: $^{31}P\{^{1}H\}$ NMR (C_6D_6, 162 MHz, 298 K) of reactivity of [Cp*Fe(d*n*ppe)Cl] with *n*-BuLi at 25 °C with a $Ph_3P{=}O$ standard.

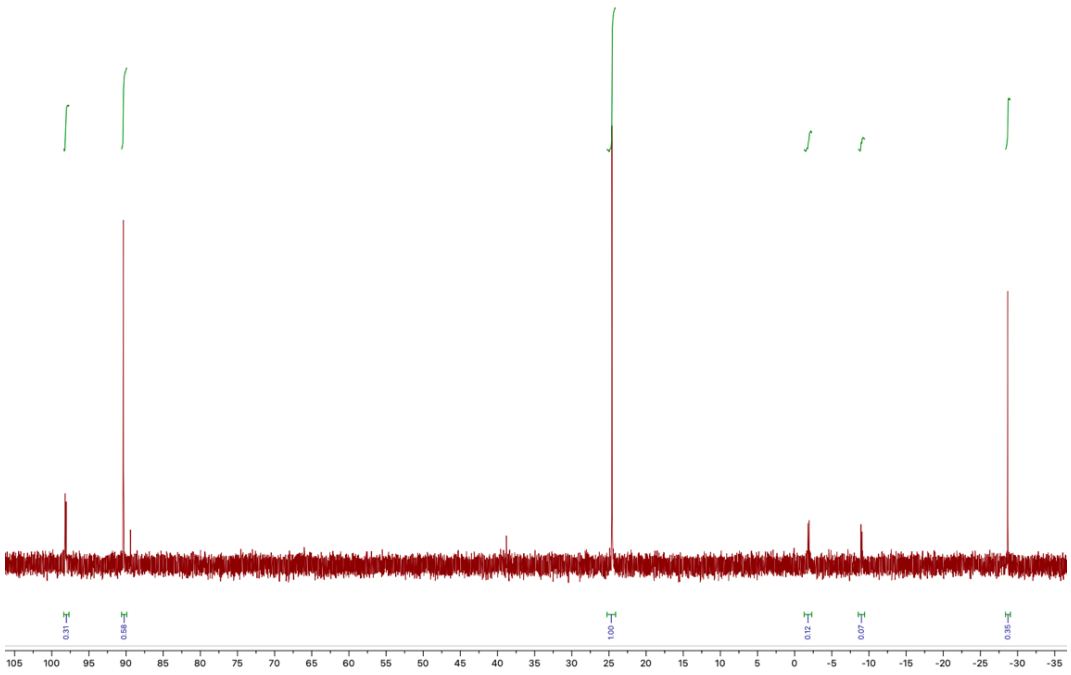

Figure S29: ^{1}H NMR (C_6D_6, 400 MHz, 298 K) of reactivity of [Cp*Fe(d*n*ppe)Cl] with *n*-BuLi at 25 °C with a $Ph_3P{=}O$ standard.

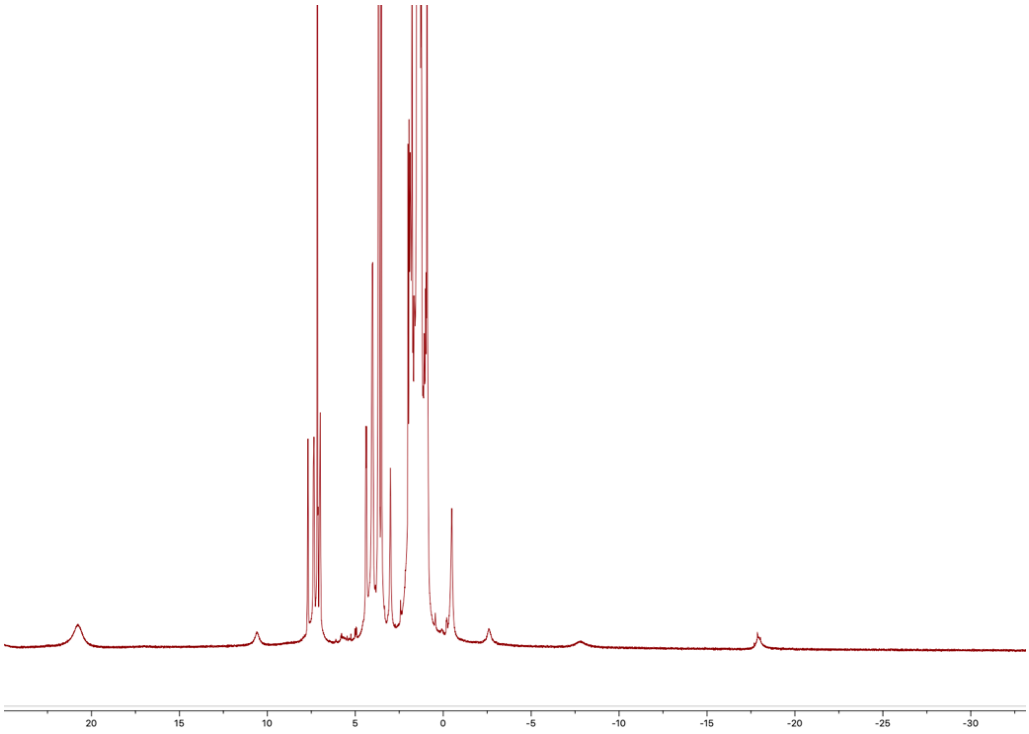

Figure S30: $^{31}P\{^{1}H\}$ NMR (C_6D_6, 162 MHz, 298 K) of reactivity of **1** with *n*BuLi at 25 °C with a $Ph_3P{=}O$ standard.

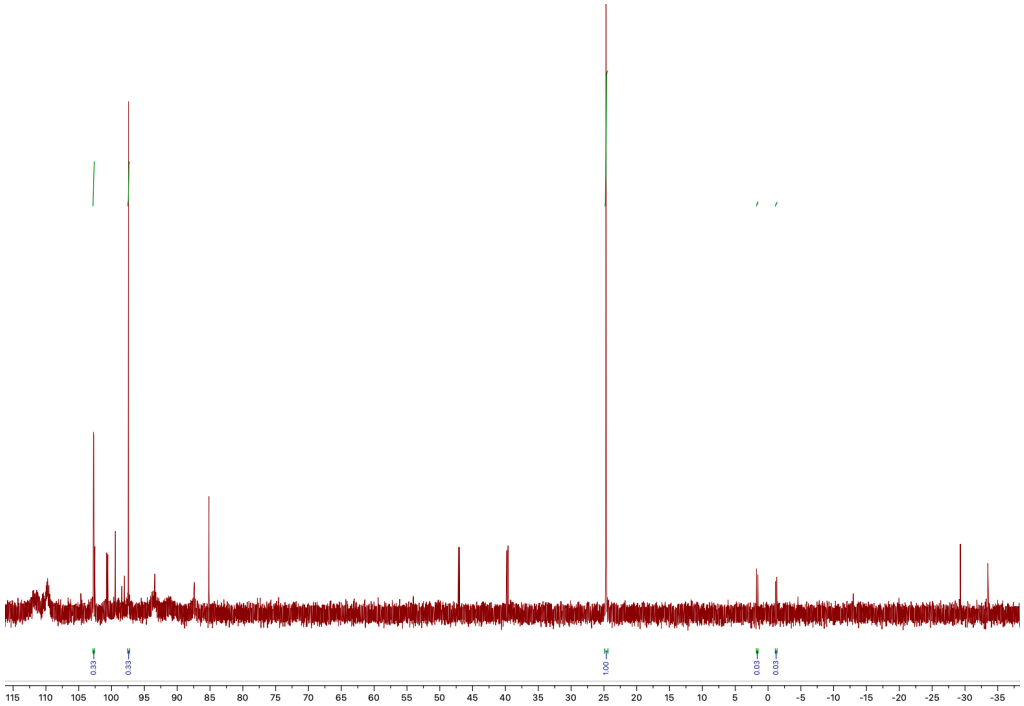

Figure S31: $^{31}P\{^{1}H\}$ NMR (C_6D_6, 162 MHz, 298 K) of compound **5** with *n*-BuLi.

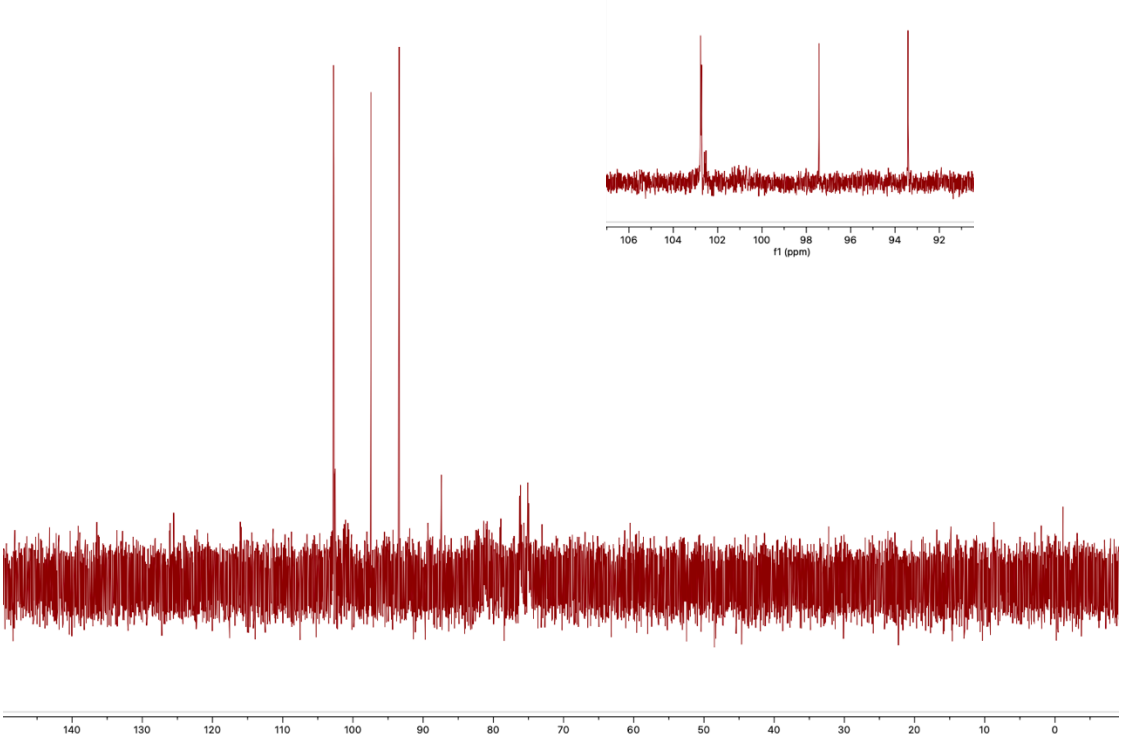

4. Decomposition Studies:

Table S1: Decomposition studies of **4** at 298 K.

Time (min)	intensity	ln(intensity)
0	0.52	-0.6539265
1300	0.21	-1.5606477
1536	0.19	-1.6607312
1791	0.18	-1.7147984
2711	0.1	-2.3025851

Figure S32: Raw data of decomposition studies displaying integration of NMR signal vs. time.

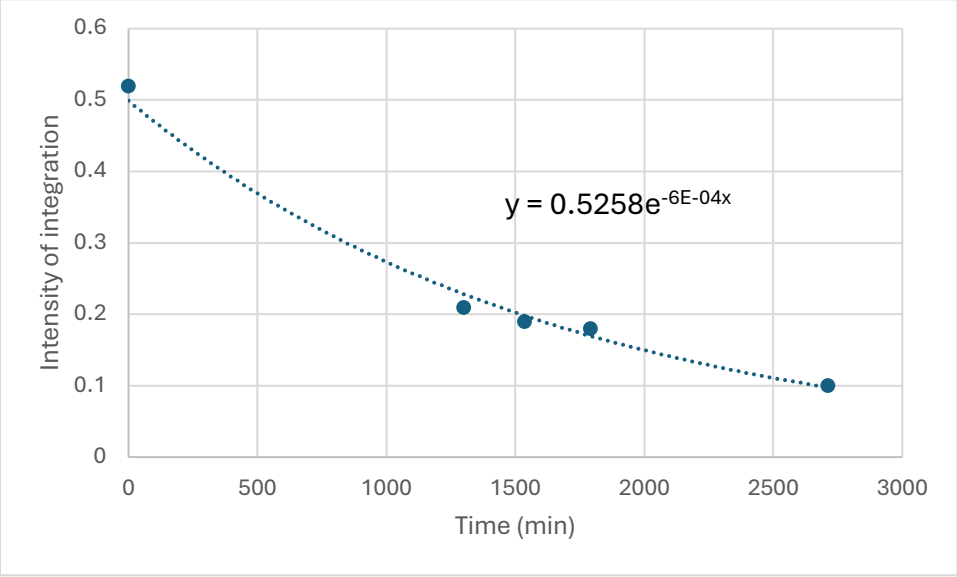

Figure S33: Natural Logarithm of NMR intensity vs. time to determine k.

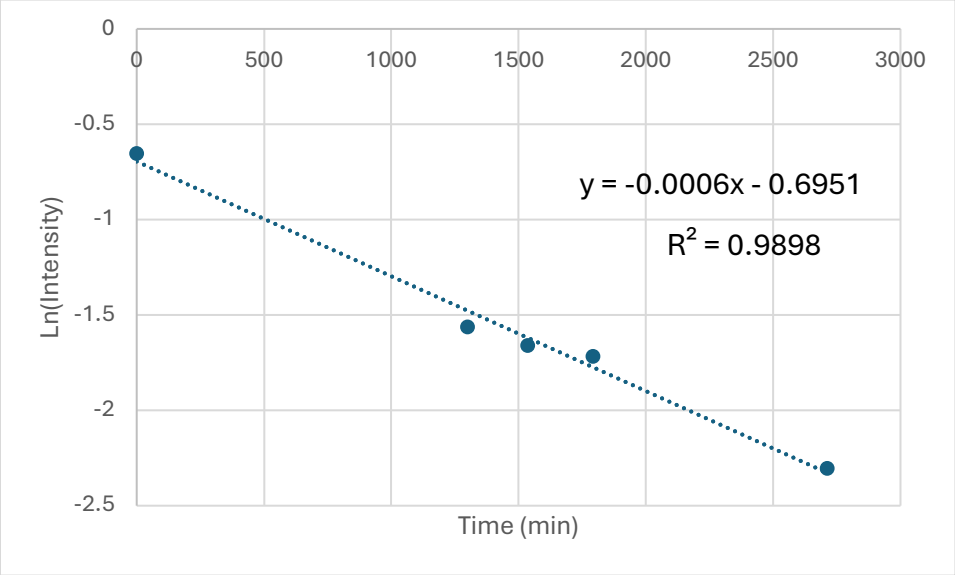

k = 0.0006

$t_{1/2} = \ln 2/k$ = 1155.2453 min

$t_{1/2}$ = 19.25 h

Figure S34: $^{31}P\{^{1}H\}$ NMR, C_6D_6, 162 MHz, 298 K. Stacked Plot of decomposition of **4** at the times listed in **Table S1** from bottom to top. (0 min, 1300 min, 1536 min, 1791 min, 2711 min).

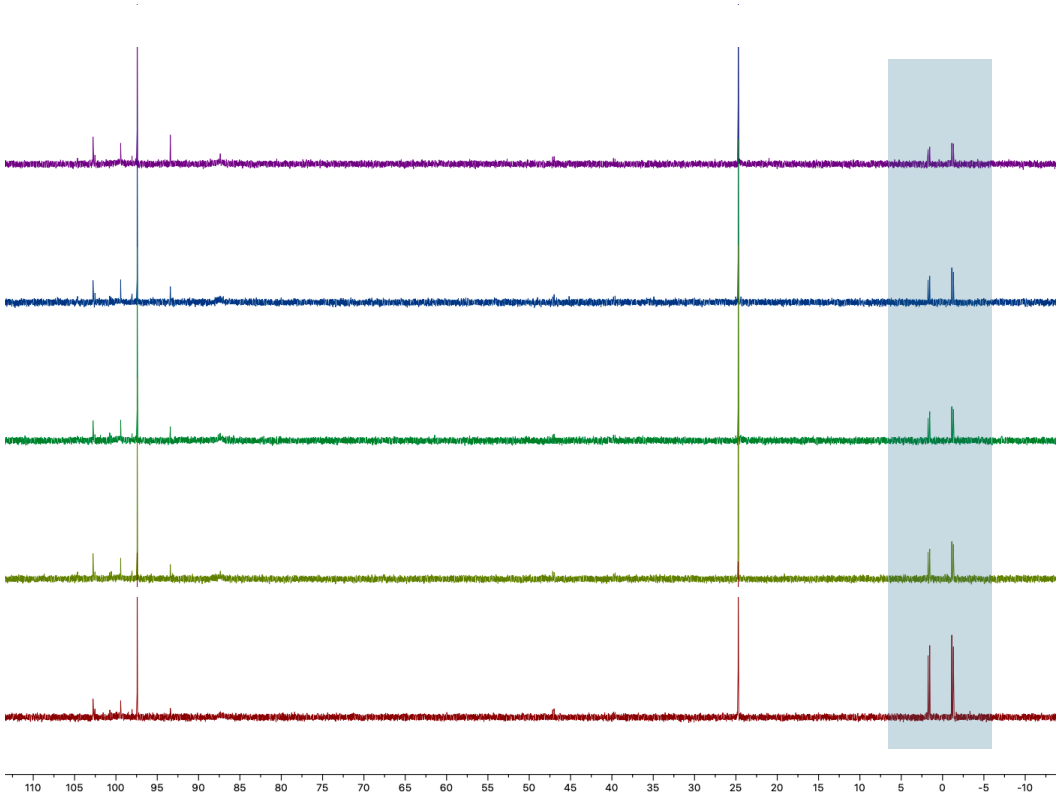

5. X-Ray Crystallography:

*Data Collection and Processing for Complex **1***:

The sample was mounted on a nylon loop with a small amount of Paratone N oil. All X-ray measurements were made on a XtaLAB Synergy, Dualflex, HyPix-Arc 100 diffractometer at a temperature of 110.00(10) K with Cu Kα, λ = 1.54184 Å radiation. The unit cell dimensions were determined from a symmetry constrained fit of 16398 reflections with 8.122° < 2θ < 152.496°. The data collection strategy was a number of ω scans which collected data up to 154.396° (2θ). Scaling and an empirical absorption correction based on spherical harmonics were applied to the data using the SCALE3 ABSPACK algorithm as implemented in CrysAlisPro (version 1.171.44.128a).[3]

*Structure Solution and Refinement for Complex **1**:*

The structure was solved using by using a dual space methodology using the SHELXT.[4] All non-hydrogen atoms were obtained from the initial solution. The hydrogen atoms were introduced at idealized positions and were allowed to ride on the parent atom. Relatively large peaks in the difference Fourier map indicated that the propyl chain was disordered over two orientations. The normalized occupancy factor for the predominant orientation converged to a value of 0.655(13). Graphic plots were produced using the Mercury program.[5]

*Data Collection and Processing for Complex **6***:

The sample was mounted on a nylon loop with a small amount of Paratone N oil. All X-ray measurements were made on a XtaLAB Synergy, Dualflex, HyPix-Arc 100 diffractometer at a temperature of 110.15 K with Cu Kα, λ = 1.54184 Å radiation. The unit cell dimensions were determined from a symmetry constrained fit of 64050 reflections with 5.712° < 2θ < 153.358°. The data collection strategy was a number of ω scans which collected data up to 153.854° (2θ). Scaling and an empirical absorption correction based on spherical harmonics were applied to the data using the SCALE3 ABSPACK algorithm as implemented in CrysAlisPro (version 1.171.44.128a).[3]

*Structure Solution and Refinement for Complex **6**:*

The structure was solved using by using a dual space methodology using the SHELXT.[4] All non-hydrogen atoms were obtained from the initial solution. The hydrogen atoms were introduced at idealized positions and were allowed to ride on the parent atom. Graphic plots were produced using the Mercury program.[5]

CCDC **2527971-2527972** contain the supplementary crystallographic data for this paper. These data can be obtained free of charge from The Cambridge Crystallographic Data Centre via www.ccdc.cam.ac.uk/data_request/cif.

Table S2: Crystallographic Data for **1** and **6**.

Identification code	**1**	**6**
Empirical formula	$C_{20}H_{39}ClFeP_2$	$C_{102}H_{150}B_2Fe_2P_6$
Formula weight	432.75	847.68
Temperature/K	110.00(10)	110.15
Crystal system	Orthorhombic	Orthorhombic
Space group	$P2_12_12_1$	$Pbca$
a/Å	8.0539(2)	17.67270(10)
b/Å	12.3788(2)	17.46570(10)
c/Å	22.5477(3)	31.0204(2)
α/°	90	90
β/°	90	90
γ/°	90	90
Volume/Å^3	2247.95(7)	9574.94(10)
Z	4	8
ρ_{calc}g/cm^3	1.279	1.176
μ/mm^{-1}	7.798	3.703
F(000)	928.0	3656.0
Crystal size/mm^3	0.17 × 0.06 × 0.04	0.14 × 0.13 × 0.05
Radiation	Cu Kα (λ = 1.54184)	CuKα (λ = 1.54184)
2Θ range for data collection/°	7.842 to 154.396	5.698 to 153.854
Index ranges	$-10 \le h \le 10$, $-15 \le k \le 15$, $-24 \le l \le 28$	$-22 \le h \le 19$, $-22 \le k \le 20$, $-39 \le l \le 38$
Reflections collected	45347	205319
Independent reflections	4719 [R_{int} = 0.0436, R_{sigma} = 0.0205]	10077 [R_{int} = 0.0397, R_{sigma} = 0.0133]
Data/restraints/parameters	4719/3/230	10077/0/512
Goodness-of-fit on F^2	1.046	1.108
Final R indexes [I>=2σ (I)]	R_1 = 0.0295, wR_2 = 0.0681	R_1 = 0.0409, wR_2 = 0.1091
Final R indexes [all data]	R_1 = 0.0307, wR_2 = 0.0686	R_1 = 0.0425, wR_2 = 0.1101
Largest diff. peak/hole / e Å^{-3}	0.47/-0.43	0.41/-0.37

Where:

$R_1 = \Sigma \mid |F_o| - |F_c| \mid / \Sigma F_o$

$wR_2 = [\Sigma(w(F_o^2 - F_c^2)^2) / \Sigma(w F_o^4)]^{½}$

GOF = $[\Sigma(w(F_o^2 - F_c^2)^2) / (\text{No. of reflns.} - \text{No. of params.})]^{½}$

6. Computational Details:

Calculations were preformed using ORCA version 6.0.1.[6] Calculations were run on the Nibi cluster maintained by compute Canada. Geometry optimizations were preformed firstly at BP86 D3BJ def2/J def2-SVP level then BP86 D3BJ def2/J def2-TZVP.[7] Convergence criteria were met using the defgrid2 integral grid size.

To obtain accurate thermochemical information, the final Gibbs free energies for each chemical species were calculated using the following equation.

$$\Delta G_{solv} = E_{el}(DLPNO\text{-}CCSD(T)) + \Delta G_{correction}(DFT) + DG^{\circ}{}_{solv}(DFT).$$

E_{el}(DLPNO-CCSD(T)) is the final electronic energy from a DLPNO-CCSD(T)/def2-TZVP calculation, $DG_{correction}$(DFT) is the G-E_{el} (Gibbs free energy minus the electronic energy) from a BP86-D3(BJ)/def2-TZVP calculation, and $\Delta G^{\circ}{}_{solv}$(DFT) is the sum of DGENP(CPCM Dielectric) and DGCDS(Free-energy(cav+disp)) from an SMD single point calculation.

To obtain NMR chemical shifts optimized geometries were utilized, and the keyword NMR was used, including %EPRNMR Nuclei = ALL P {SHIFT} or = ALL C {SHIFT} dependent on the calculated nuclei. Phosphoric acid was utilized as a phosphine NMR standard, while TMS was utilized as a carbon NMR standard.[8] Isotropic values analyzed.

To calculate chemical shifts the equation below was utilized.[9]

$$\delta_{Final} = \delta_{standard} - \delta_{calculated}\ (\text{ppm})$$

Table S3: Calculated ^{13}C NMR shifts of **4**

DFT observed Backbone Carbon Nuclei shift (ppm)	DFT observed standard TMS shift (ppm)	Chemical Shift of Nuclei (calculated) (ppm)
180.528	182.697	2.169
140.582	--	42.115

Table S4: Calculated ^{31}P NMR shifts of **4**

DFT observed Phosphorous Nuclei shift (ppm)	DFT observed standard Triphenylphosphine oxide shift	Chemical Shift of Nuclei (calculated) (ppm)
239.669	299.042	59.373
246.269	--	52.773

7. References:

(1) E. J. Palmer, R. J. Strittmatter, K. T. Thornley, J. C. Gallucci, B. E. Bursten. *Polyhedron.,* 2013, **58**, 120–128.
(2) M. W. Drover; E. G. Bowes; M. C. Dufour; L. A. Lesperance-Nantau. *Dalton Trans.* 2020, **49**, 16312–16318.
(3) Rigaku Oxford Diffraction, (2025), CrysAlisPro Software system, version 1.171.44.128a, Rigaku Corporation, Wroclaw, Poland.
(4) G.M. Sheldrick, *Acta Cryst.* 2015, **A71**, 3.
(5) C.F Macrae, I.J. Bruno, J. A. Chisholm, P.R. Edington, P. McCabe, E. Pidcock, L. Rodriguez-Monge, R. Taylor, J. van de Streek, and P. A. Wood. *J. Appl. Cryst*., 2008, **41**, 466.
(6) Neese, F. Software Update: The ORCA Program – Version 5.0. *WIREs Comput. Mol. Sci.,* 2022, **12**, e1606. (About orca)
(7) a) S. Grimme, S. Ehrlich, L. Goerigk, *J. Comput. Chem.* 2011, **32**, 1456; b) S. Grimme, J. Antony, S. Ehrlich, H. Krieg, *J. Chem. Phys.* 2010, **132**, 154104; c) F. Weigend, R. Ahlrichs, *Phys. Chem. Chem. Phys.* 2005, **7**, 3297.
(8) A. Bango, F. Rastrelli, G. Saielli, *J. Phys. Chem. A.* 2003, **107**, 9964–9973.
(9) I.L. Rusakova, Y.Y. Rusakov, *Int. J. Mol. Sci.,* 2026, **27**, 704.